Received: 1 October 2019 | Accepted: 22 April 2021

DOI: 10.1002/rnc.5565

RESEARCH ARTICLE

WILEY

Event-triggered global trajectory tracking control of a quadrotor: Synthesis, simulations, and experiments

Xuan-Zhi Zhu[1] | **Pedro Casau**[1] | **Carlos Silvestre**[1,2]

[1]Instituto Superior Técnico, Universidade de Lisboa, Lisboa, Portugal

[2]Department of Electrical and Computer Engineering, Faculty of Science and Technology, University of Macau, Macau, China

Correspondence
Xuan-Zhi Zhu, Instituto Superior Técnico, Universidade de Lisboa, 1049-001 Lisboa, Portugal.
Email: xuanzhi.zhu@tecnico.ulisboa.pt

Funding information
Fundação para a Ciência e a Tecnologia, Grant/Award Numbers: CEECIND/04652/2017, UIDB/50009/2020, UIDB/50022/2020; Fundo para o Desenvolvimento das Ciências e da Tecnologia, Grant/Award Number: FDCT/0031/2020/AFJ; Universidade de Macau, Grant/Award Number: MYRG2018-00198-FST

Abstract

This paper presents an event-triggered controller that solves the problem of trajectory tracking for an aerial vehicle with thrust actuation in a single body-fixed direction and full angular velocity actuation. Firstly, we design a globally stabilizing hybrid controller and then, using the framework of hybrid dynamical systems, we derive an appropriate event-triggering mechanism for sampling actuation signals. We prove the global asymptotic stability of a zero tracking error set for the closed-loop system. For practical implementation of the proposed event-triggered controller on digital platforms, we restrict the event-triggering condition and inflate the zero tracking error set to avoid Zeno solutions while achieving global asymptotic stability of the inflated set for the closed-loop system. The results are illustrated by numerical simulations and further verified by experiments.

KEYWORDS

event-triggered control, hybrid control systems, unmanned aerial vehicles

1 | INTRODUCTION

In recent decades, motion control of small aerial vehicles, especially quadrotors, has seen emerging techniques in an attempt to fully exploit their high maneuverability. Among different motion control tasks, the trajectory tracking problem is a fundamental one, for which there exist a variety of control strategies including proportional-integral-derivative (PID) feedback,[1] feedback linearization,[2] sliding-mode control,[3] integral backstepping,[4] adaptive control,[5] and hybrid control,[6] to name a few. Digital implementation of these controllers requires sufficiently fast periodic sampling of both measurement signals and actuation signals in order to preserve the stability of the closed-loop system. However, the requirement of a sufficiently small sampling period may not be satisfied in some circumstances, such as: limited communication bandwidth for signal transmission, transmission delay, and low computational power. Besides, it can lead to redundant samples at instants that are not actually needed to achieve the desired stability property.

The advent of event-triggered control allows less-frequent sampling while guaranteeing desired levels of performance of the closed-loop system (see the works of Åström et al.[7] and Åarzén et al.[8] for early approaches). Various Lyapunov-based event-triggering mechanisms have been proposed for the stabilization of continuous-time plants. Some rely on the existence of an input-to-state (ISS) Lyapunov function.[9-11] The work of Seuret et al.[12] removes the ISS requirement by just focusing on stabilizing the plant state. Event-triggered controllers are feasible only if it can be shown that there exists a

positive lower bound to the inter-event time. This has been achieved either by temporal regularization[13-15] or by turning off the sampling events near the set to be stabilized.[16,17]

In the context of the trajectory tracking problem of underactuated vehicles, several results achieve position and/or attitude stabilization by event-triggered control. The work of Postoyan et al.[18] presents an event-triggered feedback law for the trajectory tracking control of a planar vehicle with practical stability and provide sufficient conditions for the absence of Zeno solutions, that is, solutions with infinite jumps within finite flow time. Téllez-Guzmán et al.[19] designed an event-based LQR control strategy, derived from the results for nonlinear affine control systems,[20] for linearized attitude dynamics of a quadrotor that achieves local asymptotic stability. Similar ideas have also been applied in the design of event-triggered quaternion-based feedback laws that locally asymptotically stabilize a quadrotor around a desired fixed attitude while avoiding Zeno solutions.[21,22] A distributed event-triggered hybrid controller for leader–follower flocking for multiple quadrotors while avoiding Zeno solutions,[23] which can be identified as a position stabilization problem. Recently, it was shown that an event-triggered PID controller[24] is able to drive a quadrotor to a fixed position under the assumption that a lower bound for the sampling interval is available. However, control parameters have to be selected carefully to guarantee stability of the system due to the discretization of measured states and the local representation of the orientation by Euler-angles. In the context of networked control systems, event-triggered dual-rate control of the yaw angle for a quadrotor is achieved in the work of Cuenca et al.[25] The stability results in the aforementioned works are local, therefore limiting the possibility for inverted flight as one of the aggressive maneuvers. In fact, there is a topological obstruction to global stabilization of rotational motion by continuous feedback.[26] In light of this obstruction, we follow an approach similar to Mayhew et al.[27] in order to achieve global asymptotic stability by hybrid feedback.

In this paper, we start with the design of a control law that globally asymptotically stabilizes the position and the linear velocity dynamics, followed by backstepping, which guarantees global asymptotic stability of the zero tracking error set for the complete dynamics through hybrid feedback. Then, we develop an event-triggering mechanism on top of the given hybrid controller, that measures and enforces a given rate of decay of the Lyapunov function through sampling updates, similarly to the event-triggered implementation of a continuous-time plant in the work of Seuret et al.[12] These procedures lead to the control configuration shown in Figure 1, in which an event-triggering mechanism is devised upon the knowledge of quadrotor state $\mathbf{x}_p$ and controller state $\mathbf{x}_c$ and decides the sampling events. Between two consecutive triggering events, the quadrotor is driven by a constant (zero-order hold) actuation input $\hat{\mathbf{u}}$ whose value equals the last sample of the controller output $\mathbf{u}$.

The main contributions of this paper are: (i) proposing a control strategy for trajectory tracking of a quadrotor vehicle by synthesizing a globally stabilizing hybrid controller and an event-triggering mechanism; (ii) presenting both simulation and experimental results to demonstrate the performance of the proposed control law, where the globally asymptotically stabilizing property is tested in both upright flight as well as inverted flight (see Figure 2). In fact, the first documented experiment for stable inverted hovering appeared in the work of Michini et al.[28] and was later theoretically verified in the work of Cutler et al.[29] The main difference between their inverted flight and ours is: our quadrotor generates negative thrust by reversing the direction of motor rotation while their quadrotors do so by varying the propeller pitch angle. In addition, we exclude Zeno solutions to enable digital implementation of the proposed controller. This is achieved by restricting the set in which the event-triggering mechanism is allowed and inflating the size of the set to be stabilized. The remainder of the paper is organized as follows. Preliminary results and notation are presented in Section 2. A dynamical model for the quadrotor and the control objective are introduced in Section 3. Section 4 focuses on the design of a

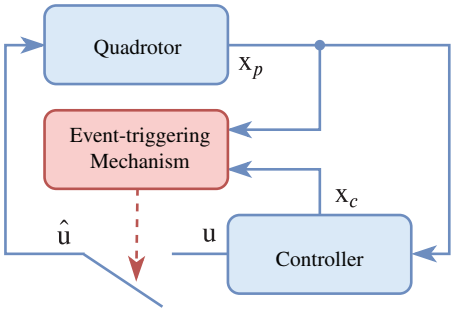

FIGURE 1 Architecture of the controlled quadrotor in closed-loop with an event-triggering mechanism on actuation signals

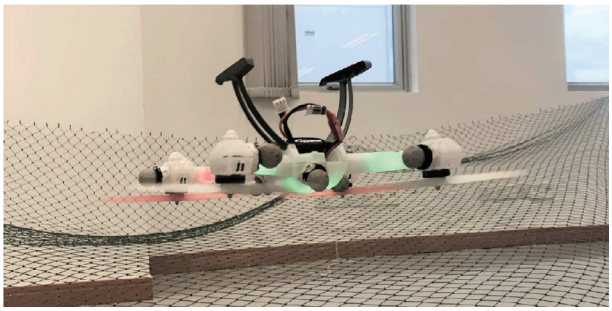

FIGURE 2 Experimental quadrotor in inverted flight

global trajectory tracking controller, followed by simulation results in Section 5and experimental results in Section 6. In Section 7, we present some concluding remarks.

2 | PRELIMINARIES

Let $\mathbb{R}$ denote the set of real numbers, $\mathbb{R}_{\geq 0} := [0, \infty[$, $\mathbb{R}_{>0} :=]0, \infty[$, $\mathbb{Z}_{\geq 0} := \{0, 1, 2, \dots\}$, $\mathbb{Z}_{>0} := \{1, 2, \dots\}$. The Euclidean n-dimensional space is denoted by $\mathbb{R}^n$, with the inner product $\langle \mathbf{x}, \mathbf{y} \rangle := \mathbf{x}^\top \mathbf{y}$ for each $\mathbf{x}, \mathbf{y} \in \mathbb{R}^n$ and the Euclidean norm $|\mathbf{x}| := \sqrt{\langle \mathbf{x}, \mathbf{x} \rangle}$ for each $\mathbf{x} \in \mathbb{R}^n$. Let $\mathbf{x} \in \mathbb{R}^n$ and $\mathbf{y} \in \mathbb{R}^m$, $(\mathbf{x}, \mathbf{y})$ stands for $\begin{bmatrix} \mathbf{x}^\top & \mathbf{y}^\top \end{bmatrix}^\top$. In $\mathbb{R}^n$, the unit vector whose ith component is 1 and the vector whose all entries equal to 0 are denoted as $\mathbf{e}_i$ and $\mathbf{0}$, respectively. Matrices in $\mathbb{R}^{m \times n}$ are represented by regular uppercase characters. In $\mathbb{R}^{n \times n}$, the identity matrix and the matrix whose all entries are equal to 0 are denoted as I_n and 0_n, respectively. The distance of a vector $\mathbf{x} \in \mathbb{R}^n$ to a set $\mathcal{A} \subset \mathbb{R}^n$ is denoted by $|\mathbf{x}|_{\mathcal{A}} := \inf\{|\mathbf{x} - \mathbf{y}| : \mathbf{y} \in \mathcal{A}\}$. The unit open ball centered at the origin is denoted as $\mathbb{B} := \{\mathbf{x} \in \mathbb{R}^n : |\mathbf{x}| < 1\}$. The unit n-sphere centered at the origin is denoted as $\mathbb{S}^n := \{\mathbf{x} \in \mathbb{R}^{n+1} : |\mathbf{x}| = 1\}$. The translation of a set $\mathcal{A} \subset \mathbb{R}^n$ by a vector $\mathbf{x} \in \mathbb{R}^n$ is denoted by $\mathbf{x} + \mathcal{A} := \{\mathbf{x} + \mathbf{y} : \mathbf{y} \in \mathcal{A}\}$. General Minkowski scalar multiples and sums of sets are defined by $\lambda \mathcal{A} := \{\lambda \mathbf{y} : \mathbf{y} \in \mathcal{A}\}$ and $\mathcal{A}_1 + \mathcal{A}_2 := \{\mathbf{y}_1 + \mathbf{y}_2 : \mathbf{y}_1 \in \mathcal{A}_1, \mathbf{y}_2 \in \mathcal{A}_2\}$, where $\lambda \in \mathbb{R}$ and $\mathcal{A}, \mathcal{A}_1, \mathcal{A}_2 \subset \mathbb{R}^n$.

Let $\mathbf{f} : \mathcal{A} \to \mathbb{R}^n$ be a differentiable function such that $\mathbf{f}(\mathbf{x}) := (f_1(\mathbf{x}), f_2(\mathbf{x}), \dots, f_n(\mathbf{x}))$ for each $\mathbf{x} \in \mathcal{A}$, where the open set $\mathcal{A} \subset \mathbb{R}^m$, the Jacobian matrix of $\mathbf{f}$ at $\mathbf{x} := (x_1, x_2, \dots, x_m) \in \mathcal{A}$ is denoted as $J_{\mathbf{f}}(\mathbf{x})$, whose (i,j)th entry $[J_{\mathbf{f}}(\mathbf{x})]_{ij} := \frac{\partial f_i}{\partial x_j}$, which reduces to the gradient if, in addition, the function is real-valued. A function $\alpha : \mathbb{R}_{\geq 0} \to \mathbb{R}_{\geq 0}$ is of class $\mathcal{K}$ if it is continuous, zero at zero, and strictly increasing; and it is of class $\mathcal{K}_\infty$ if, in addition, it is unbounded. Given a function $V : \mathcal{A} \to \mathbb{R}$ with $\mathcal{A} \subset \mathbb{R}^n$ and some $\xi \in \mathbb{R}$, let $V^{-1}(\xi) := \{\mathbf{x} \in \mathcal{A} : V(\mathbf{x}) = \xi\}$ denote its ξ-level set.

Given a set $\mathcal{A} \subset \mathbb{R}^n$, its closure is denoted as $\overline{\mathcal{A}}$ and its interior is denoted as int $\mathcal{A}$. Given a set-valued mapping $\mathcal{M} : \mathbb{R}^m \rightrightarrows \mathbb{R}^n$, the domain and the range of $\mathcal{M}$ are the sets dom $\mathcal{M} := \{\mathbf{x} \in \mathbb{R}^m : \mathcal{M}(\mathbf{x}) \neq \emptyset\}$ and rge $\mathcal{M} := \{\mathbf{y} \in \mathbb{R}^n : \exists\, \mathbf{x} \in \mathbb{R}^m, \mathbf{y} \in \mathcal{M}(\mathbf{x})\}$, respectively. Given sets $\mathcal{S} \subset \mathbb{R}^m$, we define $\mathcal{M}(\mathcal{S}) := \{\mathbf{y} \in \mathbb{R}^n : \exists\, \mathbf{x} \in \mathcal{S}, \mathbf{y} \in \mathcal{M}(\mathbf{x})\}$.

Definition 1. (See Definition 5.12 in the work of Goebel et al.[30]) The tangent cone to a set $\mathcal{A} \subset \mathbb{R}^n$ at a point $\mathbf{x} \in \mathbb{R}^n$, denoted as $\mathcal{T}_{\mathcal{A}}(\mathbf{x})$, is the set of all vectors $\mathbf{y} \in \mathbb{R}^n$ for which there exist sequences $(\mathbf{x}_i)_{i \in \mathbb{Z}_{>0}}$ and $(\tau_i)_{i \in \mathbb{Z}_{>0}}$, $\mathbf{x}_i \in \mathcal{A}$ and $\tau_i > 0$ for each $i \in \mathbb{Z}_{>0}$, with $\mathbf{x}_i \to \mathbf{x}$, $\tau_i \to 0$ as $i \to \infty$ such that $\mathbf{y} = \lim_{i \to \infty} \frac{\mathbf{x}_i - \mathbf{x}}{\tau_i}$.

We make use of hybrid systems theory that is formalized in the work of Goebel et al.[30] Under this framework, a hybrid dynamical system $\mathcal{H} := (\mathcal{F}, \mathcal{C}, \mathcal{G}, \mathcal{D})$ in $\mathbb{R}^n$ is defined as

$$\mathcal{H} : \begin{cases} \dot{\boldsymbol{\phi}} & \in \mathcal{F}(\boldsymbol{\phi}) \quad \boldsymbol{\phi} \in \mathcal{C}, \\ \boldsymbol{\phi}^+ & \in \mathcal{G}(\boldsymbol{\phi}) \quad \boldsymbol{\phi} \in \mathcal{D}, \end{cases} \tag{1}$$

where $\boldsymbol{\phi} \in \mathbb{R}^n$, $\mathcal{C} \subset \mathbb{R}^n$ is the flow set, $\mathcal{F} : \mathbb{R}^n \rightrightarrows \mathbb{R}^n$ with $\mathcal{C} \subset$ dom $\mathcal{F}$, $\mathcal{D} \subset \mathbb{R}^n$ is the jump set, and $\mathcal{G} : \mathbb{R}^n \rightrightarrows \mathbb{R}^n$ with $\mathcal{D} \subset$ dom $\mathcal{G}$. In order to facilitate the definition of solutions to (1), we introduce the concepts of hybrid time domains and hybrid arcs given next.

A subset $\mathcal{E} \subset \mathbb{R}_{\geq 0} \times \mathbb{Z}_{\geq 0}$ is a compact hybrid time domain if $\mathcal{E} = \bigcup_{j=0}^{J-1} ([t_j, t_{j+1}], j)$ for some finite sequence of times $0 = t_0 \leq t_1 \leq t_2 \leq \cdots \leq t_J$. It is a hybrid time domain if for each $(T, J) \in \mathcal{E}$, $\mathcal{E} \cap ([0, T] \times \{0, 1, \dots, J\})$ is a compact hybrid domain. A function $\boldsymbol{\phi} : \mathcal{E} \to \mathbb{R}^n$ is a hybrid arc if $\mathcal{E}$ is a hybrid time domain and if for each $j \in \mathbb{Z}_{\geq 0}$, the function $t \mapsto \boldsymbol{\phi}(t, j)$ is locally absolutely continuous on the interval $\mathcal{I}^j = \{t : (t, j) \in \mathcal{E}\}$.

A hybrid arc $\boldsymbol{\phi}$ is a solution to the hybrid system $\mathcal{H}$ if $\boldsymbol{\phi}(0,0) \in \overline{C} \cup D$, and

(*S1*) for all $j \in \mathbb{Z}_{\geq 0}$ such that $I^j = \{t : (t,j) \in \operatorname{dom} \boldsymbol{\phi}\}$ has nonempty interior,

$$\begin{aligned} &\boldsymbol{\phi}(t,j) \in C && \text{for all} && t \in \operatorname{int} I^j, \\ &\dot{\boldsymbol{\phi}}(t,j) \in F(\boldsymbol{\phi}(t,j)) && \text{for almost all} && t \in I^j; \end{aligned}$$

(*S2*) for all $(t,j) \in \operatorname{dom} \boldsymbol{\phi}$ such that $(t+1,j) \in \operatorname{dom} \boldsymbol{\phi}$,

$$\begin{aligned} \boldsymbol{\phi}(t,j) &\in D, \\ \boldsymbol{\phi}(t,j+1) &\in G(\boldsymbol{\phi}(t,j)). \end{aligned}$$

A solution $\boldsymbol{\phi}$ to $\mathcal{H}$ is maximal if there does not exist another solution $\boldsymbol{\psi}$ to $\mathcal{H}$ such that $\operatorname{dom} \boldsymbol{\phi}$ is a proper subset of $\operatorname{dom} \boldsymbol{\psi}$ and $\boldsymbol{\phi}(t,j) = \boldsymbol{\psi}(t,j)$ for each $(t,j) \in \operatorname{dom} \boldsymbol{\phi}$. A solution $\boldsymbol{\phi}$ to $\mathcal{H}$ is complete if $\operatorname{dom} \boldsymbol{\phi}$ is unbounded, and it is Zeno if, in addition, $\sup_t(\operatorname{dom} \boldsymbol{\phi}) := \sup\{t \in \mathbb{R}_{\geq 0} : \exists\, j \in \mathbb{Z}_{\geq 0}, (t,j) \in \operatorname{dom} \boldsymbol{\phi}\} < \infty$. A solution $\boldsymbol{\phi}$ to $\mathcal{H}$ is precompact if it is complete and $\overline{\operatorname{rge} \boldsymbol{\phi}}$ is compact.

We make the following definition to capture consecutive jumps.

Definition 2. Given a set-valued mapping $G : \mathbb{R}^n \rightrightarrows \mathbb{R}^n$ and a set $D \subset \mathbb{R}^n$, we define $G^1 := G$ and $G^{k+1}(\mathbf{x}) := G(D \cap G^k(\mathbf{x}))$ for each $\mathbf{x} \in \mathbb{R}^n$ and for each $k \in \mathbb{Z}_{>0}$.

We make the following definitions regarding the stability properties of a hybrid system, in view of both Definition 3.6 and Definition 7.1 in the work of Goebel et al.[30]

Definition 3. Let $\mathcal{H}$ be a hybrid system in $\mathbb{R}^n$. A closed set $\mathcal{A} \subset \mathbb{R}^n$ is said to be:

- stable for $\mathcal{H}$ if there exists a function α of class $\mathcal{K}_\infty$ such that each solution $\boldsymbol{\phi}$ to $\mathcal{H}$ satisfies $|\boldsymbol{\phi}(t,j)|_{\mathcal{A}} \leq \alpha(|\boldsymbol{\phi}(0,0)|_{\mathcal{A}})$ for each $(t,j) \in \operatorname{dom} \boldsymbol{\phi}$;
- globally attractive for $\mathcal{H}$ if each maximal solution $\boldsymbol{\phi}$ to $\mathcal{H}$ is precompact and satisfies $\lim_{t+j\to\infty} |\boldsymbol{\phi}(t,j)|_{\mathcal{A}} = 0$;
- globally asymptotically stable for $\mathcal{H}$ if it is both stable and globally attractive.

The following lemma deals with joint behavior of two set-valued mappings that evolve concurrently, offering a way to synthesize multiple hybrid dynamical systems without sacrificing the hybrid basic conditions regarding the jump sets and jump maps. Its proof is presented in Appendix A.

Lemma 1. *Given two set-valued mappings $M_1 : \mathbb{R}^n \rightrightarrows \mathbb{R}^n$ and $M_2 : \mathbb{R}^n \rightrightarrows \mathbb{R}^n$, and two sets $\mathcal{A}_1, \mathcal{A}_2 \subset \mathbb{R}^n$ that are closed relative to $\mathbb{R}^n$, if M_1 is outer semicontinuous (locally bounded) relative to $\mathcal{A}_1$ and M_2 is outer semicontinuous (locally bounded) relative to $\mathcal{A}_2$, then the set-valued mapping $M : \mathbb{R}^n \rightrightarrows \mathbb{R}^n$, given by*

$$M(\mathbf{x}) := \begin{cases} M_1(\mathbf{x}) & \mathbf{x} \in \mathcal{A}_1 \setminus \mathcal{A}_2, \\ M_2(\mathbf{x}) & \mathbf{x} \in \mathcal{A}_2 \setminus \mathcal{A}_1, \\ M_1(\mathbf{x}) \cup M_2(\mathbf{x}) & \mathbf{x} \in \mathcal{A}_1 \cap \mathcal{A}_2, \end{cases} \tag{2}$$

is outer semicontinuous (locally bounded) relative to $\mathcal{A}_1 \cup \mathcal{A}_2$.

The next lemma provides a sufficient condition for the absence of Zeno solution to a class of hybrid dynamical system, whose proof is presented in Appendix B.

Lemma 2. *Suppose that a hybrid system $\mathcal{H} := (F, C, G, D)$ in $\mathbb{R}^n$ meets the hybrid basic conditions defined in assumption 6.5 in the work of Goebel et al.[30] and there exists some $K \in \mathbb{Z}_{>0}$ such that*

$$G^K(D) \cap D = \emptyset, \tag{3}$$

where G^K is defined in Definition 2. Then each precompact solution $\boldsymbol{\phi}$ to $\mathcal{H}$ is not Zeno.

3 | PROBLEM STATEMENT

Consider a fixed orthonormal inertial frame $\{\mathcal{I}\}$ and an orthonormal body-fixed frame $\{\mathcal{B}\}$ that is attached to the center of mass of the vehicle. We follow the formulation in the work of Craig et al.[31] for the kinematics and dynamics of the rigid body vehicle given by

$$\dot{\mathbf{p}} = \mathbf{v}, \tag{4a}$$

$$\dot{\mathbf{v}} = -\frac{1}{m} RT\mathbf{e}_3 + g\mathbf{e}_3, \tag{4b}$$

$$\dot{R} = RS(\boldsymbol{\omega}), \tag{4c}$$

where $(\mathbf{p}, \mathbf{v}) \in \mathbb{R}^6$ represents the position and the linear velocity of the vehicle in $\{\mathcal{I}\}$, respectively, $R \in \mathsf{SO}(3)$ represents the rotation matrix that maps vectors in $\{\mathcal{B}\}$ to $\{\mathcal{I}\}$ with

$$\mathsf{SO}(3) := \{R \in \mathbb{R}^{3\times 3} : R^\top R = I_3, \det(R) = 1\},$$

denoting the special orthogonal group of order 3, the mapping S is such that

$$S(\mathbf{a}) := \begin{bmatrix} 0 & -a_3 & a_2 \\ a_3 & 0 & -a_1 \\ -a_2 & a_1 & 0 \end{bmatrix},$$

for each $\mathbf{a} := (a_1, a_2, a_3) \in \mathbb{R}^3$, $\boldsymbol{\omega} \in \mathbb{R}^3$ represents the angular velocity of the vehicle in $\{\mathcal{B}\}$, $m \in \mathbb{R}_{>0}$ represents the mass of the vehicle, $T \in \mathbb{R}$ represents the thrust, $g \in \mathbb{R}_{>0}$ represents the local gravitational acceleration. In (4b), we define $\mathbf{r}_3 := R\mathbf{e}_3 \in \mathbb{S}^2$ for each $R \in \mathsf{SO}(3)$, which aligns with the thrust direction in $\{\mathcal{I}\}$. Manipulation of (4) gives rise to the following set of differential equations.

$$\dot{\mathbf{p}} = \mathbf{v}, \tag{5a}$$

$$\dot{\mathbf{v}} = -\frac{1}{m} \mathbf{r}_3 T + g\mathbf{e}_3, \tag{5b}$$

$$\dot{\mathbf{r}}_3 = -S(\mathbf{r}_3)\breve{\boldsymbol{\omega}}, \tag{5c}$$

where and $\breve{\boldsymbol{\omega}} := R\boldsymbol{\omega}$ defines the angular velocity of the vehicle in $\{\mathcal{I}\}$.

A reference trajectory is a precompact solution $t \mapsto \mathbf{r}(t) := (\mathbf{p}_d(t), \dot{\mathbf{p}}_d(t), \ddot{\mathbf{p}}_d(t))$ for each $t \in \mathbb{R}_{\geq 0}$ to the differential inclusion

$$\dot{\mathbf{r}} \in \mathcal{F}_d(\mathbf{r}) := \left\{ \mathbf{f}_d\left(\mathbf{r}, \mathbf{p}_d^{(3)}\right) : \mathbf{p}_d^{(3)} \in r\overline{\mathbb{B}} \right\},$$

where $r \in \mathbb{R}_{>0}$ and $\mathbf{f}_d\left(\mathbf{r}, \mathbf{p}_d^{(3)}\right) := \left(\dot{\mathbf{p}}_d, \ddot{\mathbf{p}}_d, \mathbf{p}_d^{(3)}\right)$ for each $\left(\mathbf{r}, \mathbf{p}_d^{(3)}\right) \in \mathbb{R}^6 \times r\overline{\mathbb{B}}$, therefore rge $\mathbf{r} \subset \mathcal{S}_d$ for some compact set $\mathcal{S}_d \subset \mathbb{R}^9$, and the set-valued mapping $\mathcal{F}_d(\mathbf{r})$ satisfies*

$$\mathcal{F}_d(\mathbf{r}) \cap \mathcal{T}_{\mathcal{S}_d}(\mathbf{r}) \neq \emptyset, \tag{6}$$

for each $\mathbf{r} \in \mathcal{S}_d$, where we recall $\mathcal{T}_{\mathcal{S}_d}(\mathbf{r})$ is the tangent cone to the set $\mathcal{S}_d$ at $\mathbf{r} \in \mathbb{R}^9$, see Definition (1). Such observation is crucial in proving completeness of maximal solutions to a hybrid system. Moreover, we make the following assumption in order to prevent reference trajectories whose acceleration equals the local gravitational acceleration:

*Equation (6) follows from lemma 5.26 in the work of Goebel et al.[30] by continuity of $\mathbf{f}_d$, compactness and convexity of $r\overline{\mathbb{B}}$, implying outer semicontinuity and local boundedness of $\mathcal{F}_d$ relative to $\mathcal{S}_d$.

Assumption 1. The set S_d satisfies $\sup_{\mathbf{r}\in S_d}|\ddot{\mathbf{p}}_d| < g$. □

Under the aforementioned definitions, we define the problem statement as follows.

Problem Statement. To design an event-triggered controller that globally asymptotically stabilizes a reference trajectory satisfying Assumption 1 for the dynamical system (5).

4 | CONTROLLER DESIGN

4.1 | Global asymptotic stabilization of both the position and the linear velocity dynamics

In this section, we design a feedback control law for both the position and the linear velocity error system given a reference trajectory $\mathbf{r} = (\mathbf{p}_d, \dot{\mathbf{p}}_d, \ddot{\mathbf{p}}_d)$. We define the position and the linear velocity tracking errors as follows

$$\begin{aligned}\mathbf{z}_1 &:= \mathbf{p} - \mathbf{p}_d,\\ \mathbf{z}_2 &:= \mathbf{v} - \dot{\mathbf{p}}_d,\end{aligned}$$

whose time derivatives are given by

$$\dot{\mathbf{z}}_1 = \mathbf{z}_2, \tag{7a}$$

$$\dot{\mathbf{z}}_2 = -\frac{1}{m}\mathbf{r}_3 T + g\mathbf{e}_3 - \ddot{\mathbf{p}}_d, \tag{7b}$$

which can be regarded as a system driven by the *virtual input* $\mathbf{r}_3 T$. Let $\mathbf{z} := (\mathbf{z}_1, \mathbf{z}_2)$ and

$$\boldsymbol{\mu}(\mathbf{r}, \mathbf{z}) := \boldsymbol{\beta}(\boldsymbol{\kappa}(\mathbf{z})) + g\mathbf{e}_3 - \ddot{\mathbf{p}}_d,$$

for each $(\mathbf{r}, \mathbf{z}) \in S_d \times \mathbb{R}^6$, where

$$\boldsymbol{\kappa}(\mathbf{z}) := k_{\mathbf{p}}\mathbf{z}_1 + k_{\mathbf{v}}\mathbf{z}_2, \tag{8}$$

for each $\mathbf{z} \in \mathbb{R}^6$, $k_{\mathbf{p}}, k_{\mathbf{v}} \in \mathbb{R}_{>0}$, and the saturation function $\boldsymbol{\beta} : \mathbb{R}^3 \to \mathbb{R}^3$ is such that $\boldsymbol{\beta}(\boldsymbol{\xi}) := (\beta_1(\xi_1), \beta_2(\xi_2), \beta_3(\xi_3))$ for each $\boldsymbol{\xi} := (\xi_1, \xi_2, \xi_3) \in \mathbb{R}^3$, with $\beta_i : \mathbb{R} \to \mathbb{R}$ continuously differentiable and verifying

$$0 < \nabla\beta_i(\xi) \leq M_{\beta_i} \quad \text{for each} \quad \xi \in \mathbb{R}, \tag{9a}$$

$$\beta_i(0) = 0, \tag{9b}$$

$$\lim_{\xi\to\pm\infty}\beta_i(\xi) = \pm K_{\beta_i} \tag{9c}$$

for some $M_{\boldsymbol{\beta}} := (M_{\beta_1}, M_{\beta_2}, M_{\beta_3})$, $K_{\boldsymbol{\beta}} := (K_{\beta_1}, K_{\beta_2}, K_{\beta_3}) \in \mathbb{R}_{>0} \times \mathbb{R}_{>0} \times \mathbb{R}_{>0}$ and for each $i \in \{1, 2, 3\}$.

Lemma 3. *Suppose Assumption 1 holds, let $K_{\boldsymbol{\beta}} \in \mathbb{R}_{>0} \times \mathbb{R}_{>0} \times \mathbb{R}_{>0}$ be such that*

$$|K_{\boldsymbol{\beta}}| < g - \sup_{\mathbf{r}\in S_d}|\ddot{\mathbf{p}}_d|, \tag{10}$$

then for each $(\mathbf{r}, \mathbf{z}) \in S_d \times \mathbb{R}^6$, $|\boldsymbol{\mu}(\mathbf{r}, \mathbf{z})| > 0$.

Proof. Using the reverse triangular inequality, it follows from the properties of the saturation function $\boldsymbol{\beta}$ that $|\boldsymbol{\mu}(\mathbf{r}, \mathbf{z})| = |\boldsymbol{\beta}(\boldsymbol{\kappa}(\mathbf{z})) + g\mathbf{e}_3 - \ddot{\mathbf{p}}_d| \geq g - |\boldsymbol{\beta}(\boldsymbol{\kappa}(\mathbf{z}))| - |\ddot{\mathbf{p}}_d| \geq g - |K_{\boldsymbol{\beta}}| - |\ddot{\mathbf{p}}_d|$, which holds for each $(\mathbf{r}, \mathbf{z}) \in S_d \times \mathbb{R}^6$. As the inequality (10) holds, it is guaranteed that $|\boldsymbol{\mu}(\mathbf{r}, \mathbf{z})| > 0$ for each $(\mathbf{r}, \mathbf{z}) \in S_d \times \mathbb{R}^6$. ■

Remark 1. In fact, there always exist a $K_\beta \in \mathbb{R}_{>0} \times \mathbb{R}_{>0} \times \mathbb{R}_{>0}$ satisfying the inequality (10) under Assumption 1.

We define the desired direction $\mathbf{r}_{3d}$ as

$$\mathbf{r}_{3d}(\mathbf{r}, \mathbf{z}) := \frac{\boldsymbol{\mu}(\mathbf{r}, \mathbf{z})}{|\boldsymbol{\mu}(\mathbf{r}, \mathbf{z})|}, \tag{11}$$

for each $(\mathbf{r}, \mathbf{z}) \in \mathcal{S}_d \times \mathbb{R}^6$ and a feedback control law for the thrust T as

$$T(\mathbf{r}, \mathbf{z}, \mathbf{r}_3) := m\mathbf{r}_3^\top \boldsymbol{\mu}(\mathbf{r}, \mathbf{z}), \tag{12}$$

for each $(\mathbf{r}, \mathbf{z}, \mathbf{r}_3) \in \mathcal{S}_d \times \mathbb{R}^6 \times \mathbb{S}^2$. We make a remark here that (11) is continuous as long as Assumption 1 holds, since we can always select a K_β satisfying (10) under Assumption 1.

By assigning the functions defined in (11) and (12) to the *virtual input* in (7b), that is, $\mathbf{r}_3 T = \mathbf{r}_{3d}(\mathbf{r}, \mathbf{z}) T(\mathbf{r}, \mathbf{z}, \mathbf{r}_{3d}(\mathbf{r}, \mathbf{z}))$, we obtain the following closed-loop system

$$\dot{\mathbf{z}}_1 = \mathbf{z}_2, \tag{13a}$$

$$\dot{\mathbf{z}}_2 = -\boldsymbol{\beta}(\boldsymbol{\kappa}(\mathbf{z})), \tag{13b}$$

whose stability is studied in the work of Casau et al.[32] but is reproduced in the following to make this paper self-contained. We first examine a Lyapunov function candidate given in the lemma below, whose proof is presented in Appendix C.

Lemma 4. *Consider the function* $\overline{V} : \mathbb{R}^6 \to \mathbb{R}$, *given by*

$$\overline{V}(\mathbf{z}) := \sum_{i=1}^{3} \left(\frac{1}{2} \begin{bmatrix} \beta_i(\kappa_i(\mathbf{z})) \\ \mathbf{e}_i^\top \mathbf{z}_2 \end{bmatrix}^\top D \begin{bmatrix} \beta_i(\kappa_i(\mathbf{z})) \\ \mathbf{e}_i^\top \mathbf{z}_2 \end{bmatrix} + \int_0^{\kappa_i(\mathbf{z})} \beta_i(\tau) d\tau \right), \tag{14}$$

where $\kappa_i(\mathbf{z}) := \mathbf{e}_i^\top \boldsymbol{\kappa}(\mathbf{z})$ *for each* $\mathbf{z} \in \mathbb{R}^6$ *and for each* $i \in \{1, 2, 3\}$, $D := \begin{bmatrix} \frac{k_\mathbf{v}}{k_\mathbf{p}}\gamma & -\gamma \\ -\gamma & k_\mathbf{p} \end{bmatrix}$ *with* $\gamma \in]0, k_\mathbf{v}[$. *Then* $\overline{V}$ *is positive definite relative to the origin and radially unbounded. Moreover, the time derivative of* $\overline{V}$ *evaluated along the solution to the differential Equations (13), given by*

$$\left\langle \nabla \overline{V}(\mathbf{z}), \begin{bmatrix} \mathbf{z}_2 \\ -\boldsymbol{\beta}(\boldsymbol{\kappa}(\mathbf{z})) \end{bmatrix} \right\rangle := -\overline{W}(\mathbf{z}), \tag{15}$$

for each $\mathbf{z} \in \mathbb{R}^6$, *is negative definite relative to the origin.*

Taking $\overline{V}$ in (14), it follows from theorem 4.2 in the work of Khalil et al.[33] that the origin is globally asymptotically stable for the system (13).

4.2 | Global asymptotic stabilization of (5) by hybrid feedback

Building on the controller in Section 4.1, we first develop a feedback control law for the angular velocity and then make it globally asymptotically stabilize the complete dynamics by means of hybrid feedback.

From now on, we take into account the attitude kinematics. The error system consisting of (5c) and (7), driven by T and $\breve{\boldsymbol{\omega}}$, is written as

$$\begin{bmatrix} \dot{\mathbf{z}} \\ \dot{\mathbf{r}}_3 \end{bmatrix} = \begin{bmatrix} \mathbf{z}_2 \\ -\frac{1}{m}\mathbf{r}_3 T + g\mathbf{e}_3 - \ddot{\mathbf{p}}_d \\ -S(\mathbf{r}_3)\breve{\boldsymbol{\omega}} \end{bmatrix} =: \mathbf{f}(\mathbf{r}, \mathbf{z}, \mathbf{r}_3, T, \breve{\boldsymbol{\omega}}),$$

where the function $\mathbf{f}$ is defined for each $(\mathbf{r}, \mathbf{z}, \mathbf{r}_3, T, \check{\boldsymbol{\omega}}) \in \mathcal{S}_d \times \mathbb{R}^6 \times \mathbb{S}^2 \times \mathbb{R} \times \mathbb{R}^3$.

For global asymptotic tracking of the reference trajectory, we employ synergistic hybrid feedback[27] to overcome the topological obstruction to global stabilization of rotational motion, $\mathbf{r}_3$ in our case, by continuous state feedback.[26] In this direction, we make use of a logic variable $q \in \mathcal{Q} := \{-1, 1\}$, define $\mathbf{x}_0 := (\mathbf{r}, \mathbf{z}, \mathbf{r}_3, q)$, and choose a new Lyapunov function candidate

$$V_q(\mathbf{r}, \mathbf{z}, \mathbf{r}_3) := \overline{V}(\mathbf{z}) + \epsilon \left(1 - q\mathbf{r}_3^\top \mathbf{r}_{3d}(\mathbf{r}, \mathbf{z})\right), \tag{16}$$

for each $\mathbf{x}_0 \in \mathbb{R}^{19}$, which is continuously differentiable on some open set containing the set

$$\mathcal{S}_{\mathbf{x}_0} := \mathcal{S}_d \times \mathbb{R}^6 \times \mathbb{S}^2 \times \mathcal{Q},$$

where $\overline{V}$ is defined in (14) and $\epsilon \in \mathbb{R}_{>0}$.

Following a backstepping approach, a feedback law for the angular velocity can be chosen as

$$\check{\boldsymbol{\omega}}\left(\mathbf{x}_0, \mathbf{p}_d^{(3)}\right) := \frac{1}{q\epsilon} |\boldsymbol{\mu}(\mathbf{r}, \mathbf{z})| S(\mathbf{r}_3) \begin{bmatrix} 0_3 \\ I_3 \end{bmatrix}^\top \nabla \overline{V}(\mathbf{z}) + \frac{k_{\boldsymbol{\omega}}}{q} S(\mathbf{r}_3)\, \mathbf{r}_{3d}(\mathbf{r}, \mathbf{z}) + \check{\boldsymbol{\omega}}_d\left(\mathbf{r}, \mathbf{z}, \mathbf{r}_3, \mathbf{p}_d^{(3)}\right), \tag{17}$$

for each $\left(\mathbf{x}_0, \mathbf{p}_d^{(3)}\right) \in \mathcal{S}_{\mathbf{x}_0} \times r\overline{\mathbb{B}}$, where $k_{\boldsymbol{\omega}} \in \mathbb{R}_{>0}$, the first term counteracts the position and linear velocity errors, the second term penalizes the deviation of $\mathbf{r}$ from $\mathbf{r}_{3d}$, the third term represents the desired angular velocity given by

$$\check{\boldsymbol{\omega}}_d\left(\mathbf{r}, \mathbf{z}, \mathbf{r}_3, \mathbf{p}_d^{(3)}\right) := \frac{S(\mathbf{r}_{3d}(\mathbf{r}, \mathbf{z}))}{|\boldsymbol{\mu}(\mathbf{r}, \mathbf{z})|} \left(J_{\boldsymbol{\beta}}(\boldsymbol{\kappa}(\mathbf{z})) \left(k_{\mathbf{p}}\mathbf{z}_2 - k_{\mathbf{v}} \left(\boldsymbol{\beta}(\boldsymbol{\kappa}(\mathbf{z})) + S(\mathbf{r}_3)^2 \boldsymbol{\mu}(\mathbf{r}, \mathbf{z})\right)\right) - \mathbf{p}_d^{(3)}\right), \tag{18}$$

for each $\left(\mathbf{r}, \mathbf{z}, \mathbf{r}_3, \mathbf{p}_d^{(3)}\right) \in \mathcal{S}_d \times \mathbb{R}^6 \times \mathbb{S}^2 \times r\overline{\mathbb{B}}$, where we recall $J_{\boldsymbol{\beta}}(\boldsymbol{\kappa}(\mathbf{z}))$ is the Jacobian matrix of the saturation function $\boldsymbol{\beta}$ evaluated at $\boldsymbol{\kappa}(\mathbf{z})$, the deduction of (18) detailed in Appendix D.

To represent the closed-loop dynamics driven by the feedback control laws (12) and (17), we define

$$\mathbf{f}_0\left(\mathbf{x}_0, \mathbf{p}_d^{(3)}\right) := \begin{bmatrix} \mathbf{f}_d\left(\mathbf{r}, \mathbf{p}_d^{(3)}\right) \\ \mathbf{f}\left(\mathbf{r}, \mathbf{z}, \mathbf{r}_3, T(\mathbf{r}, \mathbf{z}, \mathbf{r}_3), \check{\boldsymbol{\omega}}\left(\mathbf{x}_0, \mathbf{p}_d^{(3)}\right)\right) \\ 0 \end{bmatrix}, \tag{19}$$

for each $\left(\mathbf{x}_0, \mathbf{p}_d^{(3)}\right) \in \mathcal{S}_{\mathbf{x}_0} \times r\overline{\mathbb{B}}$ such that the time derivative of $\mathbf{x}_0 \mapsto V_q(\mathbf{r}, \mathbf{z}, \mathbf{r}_3)$ evaluated along the solution to the differential Equation (19) is obtained as

$$W(\mathbf{r}, \mathbf{z}, \mathbf{r}_3) := \left\langle \nabla V_q(\mathbf{r}, \mathbf{z}, \mathbf{r}_3), \mathbf{f}_0\left(\mathbf{x}_0, \mathbf{p}_d^{(3)}\right)\right\rangle = -\overline{W}(\mathbf{z}) - \epsilon k_{\boldsymbol{\omega}} |S(\mathbf{r}_3)\, \mathbf{r}_{3d}(\mathbf{r}, \mathbf{z})|^2, \tag{20}$$

for each $(\mathbf{r}, \mathbf{z}, \mathbf{r}_3) \in \mathcal{S}_d \times \mathbb{R}^6 \times \mathbb{S}^2$, where $\overline{W}$ is defined in (15). We note that W equals zero if and only if $(\mathbf{z}, \mathbf{r}_3) = \left(\mathbf{0}, \pm \frac{g\mathbf{e}_3 - \ddot{\mathbf{p}}_d}{|g\mathbf{e}_3 - \ddot{\mathbf{p}}_d|}\right)$, or more subtly $(\mathbf{z}, \mathbf{r}_3, q) = \left(\mathbf{0}, q\frac{g\mathbf{e}_3 - \ddot{\mathbf{p}}_d}{|g\mathbf{e}_3 - \ddot{\mathbf{p}}_d|}, \pm 1\right)$. Now consider the definition

$$\mathcal{A}_0 := \left\{ \mathbf{x}_0 \in \mathcal{S}_{\mathbf{x}_0} : \mathbf{z} = \mathbf{0}, \mathbf{r}_3 = q\frac{g\mathbf{e}_3 - \ddot{\mathbf{p}}_d}{|g\mathbf{e}_3 - \ddot{\mathbf{p}}_d|} \right\}, \tag{21}$$

with $q \in \mathcal{Q}$. From a physical point of view, $\mathcal{A}_0$ corresponds to zero tracking error during upright/inverted flight, explained in the sequel. From (10) we know that the third component of $\mathbf{r}_{3d}$, defined in (11), is positive throughout time, thus $q = 1$ implies that the vector $q\mathbf{r}_{3d}$ will stay within the hemisphere of $\mathbb{S}^2$ in which the vector has positive projection along the z-axis in inertial frame. Meanwhile, $q = -1$ implies that the vector will stay within the other hemisphere. If we choose the z-axis of the inertial frame to point downwards to the ground, then $q = 1$ denotes upright flight while $q = -1$ denotes inverted flight. From a mathematical point of view, the introduction of the variable q in the definition of $\mathcal{A}_0$ leads to a

family of potential functions on $\mathbb{S}^2$ that is synergistic with gap exceeding η (see the work of Mayhew et al.[27]). This allows for global asymptotic stabilization of a desired orientation on $\mathbb{S}^2$ by hybrid feedback, a task not achievable by continuous feedback.

For global asymptotic stabilization of $\mathcal{A}_0$, we define the the hybrid system $\mathcal{H}_0 := (\mathcal{F}_0, \mathcal{C}_0, \mathcal{G}_0, \mathcal{D}_0)$ given by

$$\mathcal{H}_0 : \begin{cases} \dot{\mathbf{x}}_0 \in \mathcal{F}_0(\mathbf{x}_0) := \left\{ \mathbf{f}_0\left(\mathbf{x}_0, \mathbf{p}_d^{(3)}\right) : \mathbf{p}_d^{(3)} \in r\overline{\mathbb{B}} \right\} & \mathbf{x}_0 \in \mathcal{C}_0 := \left\{ \mathbf{x}_0 \in \mathcal{S}_{\mathbf{x}_0} : \Delta(\mathbf{x}_0) \leq \eta \right\}, \\ \mathbf{x}_0^+ \in \mathcal{G}_0(\mathbf{x}_0) := (\mathbf{r}, \mathbf{z}, \mathbf{r}_3, -q) & \mathbf{x}_0 \in \mathcal{D}_0 := \left\{ \mathbf{x}_0 \in \mathcal{S}_{\mathbf{x}_0} : \Delta(\mathbf{x}_0) \geq \eta \right\}, \end{cases} \tag{22}$$

where dom $\mathcal{F}_0 =$ dom $\mathcal{G}_0 = \mathcal{S}_{\mathbf{x}_0}$, $\eta \in]0, 2\epsilon[$, and

$$\Delta(\mathbf{x}_0) := V_q(\mathbf{r}, \mathbf{z}, \mathbf{r}_3) - \min_{\rho \in Q} V_\rho(\mathbf{r}, \mathbf{z}, \mathbf{r}_3),$$

for each $\mathbf{x}_0 \in \mathcal{S}_{\mathbf{x}_0}$, such that $\{V_q\}_{q \in Q}$ is synergistic with synergy gap exceeding η (see the work of Mayhew et al.[27] for detail). Based on hybrid feedback given in (22), stability of a zero tracking error set for $\mathcal{H}_0$ can be guaranteed, as shown by the next result with its proof presented in Appendix E.

Lemma 5. *Suppose Assumption 1 holds, then the set $\mathcal{A}_0$ defined in (21) is globally asymptotically stable for the hybrid system $\mathcal{H}_0$ defined by (22).*

4.3 | Event-triggered implementation of the hybrid controller in Section 4.2

Now, we consider the effect of sampling of actuation signals, namely synchronized sampling of both thrust T and the angular velocity $\check{\boldsymbol{\omega}}$, resulting from zero-order-hold devices. We denote the sampled thrust and the sampled angular velocity as s_1 and $\mathbf{s}_2$, respectively. In this way, $(s_1, \mathbf{s}_2)$ is updated to the value of $(T, \check{\boldsymbol{\omega}})$ at some $\left(\mathbf{x}_0, \mathbf{p}_d^{(3)}\right)$ under certain event-triggering mechanism, and remains constant otherwise. We resort to an event-triggering mechanism proposed in the work of Seuret et al.,[12] that monitors and enforces a given rate of decay of the Lyapunov function (16), in an attempt to avoid continuous sampling of $(s_1, \mathbf{s}_2)$. Under such a mechanism, however, the occurrence of an update of $(s_1, \mathbf{s}_2)$ may coincide with that of a jump of the variable q in (22). This concern is addressed by considering their joint behavior as formalized in (2). In this direction, we define $\mathbf{x} := (\mathbf{x}_0, s_1, \mathbf{s}_2)$ and consider the following the hybrid system $\mathcal{H} := (\mathcal{F}, \mathcal{C}, \mathcal{G}, \mathcal{D})$ given by

$$\mathcal{H} : \begin{cases} \dot{\mathbf{x}} \in \mathcal{F}(\mathbf{x}) := \left\{ \begin{bmatrix} \mathbf{f}_d\left(\mathbf{r}, \mathbf{p}_d^{(3)}\right) \\ \mathbf{f}(\mathbf{r}, \mathbf{z}, \mathbf{r}_3, s_1, \mathbf{s}_2) \\ \mathbf{0} \end{bmatrix} : \mathbf{p}_d^{(3)} \in r\overline{\mathbb{B}} \right\} & \mathbf{x} \in \mathcal{C} := \mathcal{C}_1 \cap \mathcal{C}_2, \\ \mathbf{x}^+ \in \mathcal{G}(\mathbf{x}) := \mathcal{G}_1(\mathbf{x}) \cup \mathcal{G}_2(\mathbf{x}) & \mathbf{x} \in \mathcal{D} := \mathcal{D}_1 \cup \mathcal{D}_2, \end{cases} \tag{23}$$

where dom $\mathcal{F} = \mathcal{S}_{\mathbf{x}} := \mathcal{S}_{\mathbf{x}_0} \times \mathbb{R} \times \mathbb{R}^3$, dom $\mathcal{G} = \mathcal{D}$, $\mathcal{C}_1 := \mathcal{C}_0 \times \mathbb{R} \times \mathbb{R}^3$, $\mathcal{D}_1 := \mathcal{D}_0 \times \mathbb{R} \times \mathbb{R}^3$,

$$\mathcal{C}_2 := \left\{ \mathbf{x} \in \mathcal{S}_{\mathbf{x}} : \max_{\mathbf{u} \in \mathcal{F}(\mathbf{x})} \left\langle \nabla \widetilde{V}_q(\mathbf{x}), \mathbf{u} \right\rangle \leq \sigma \widetilde{W}(\mathbf{x}) \right\},$$
$$\mathcal{D}_2 := \left\{ \mathbf{x} \in \mathcal{S}_{\mathbf{x}} : \max_{\mathbf{u} \in \mathcal{F}(\mathbf{x})} \left\langle \nabla \widetilde{V}_q(\mathbf{x}), \mathbf{u} \right\rangle \geq \sigma \widetilde{W}(\mathbf{x}) \right\},$$

where the function $\mathbf{x} \mapsto \widetilde{V}_q(\mathbf{x})$ is an extension of the function (16) such that $\widetilde{V}_q(\mathbf{x}) = V_q(\mathbf{r}, \mathbf{z}, \mathbf{r}_3)$ for each $\mathbf{x} \in \mathbb{R}^{23}$ and is continuously differentiable on some open set containing $\mathcal{S}_{\mathbf{x}}$, the function $\mathbf{x} \mapsto \widetilde{W}(\mathbf{x})$ is an extension of the function (20) such that $\widetilde{W}(\mathbf{x}) = W(\mathbf{r}, \mathbf{z}, \mathbf{r}_3)$ for each $\mathbf{x} \in \mathcal{S}_{\mathbf{x}}$, and $\sigma \in]0, 1[$, which is referred to as *the sampling tuning factor* that allows some flow time for sampling. The map

$$\mathcal{G}_1(\mathbf{x}) := (\mathcal{G}_0(\mathbf{x}_0), s_1, \mathbf{s}_2), \tag{24}$$

where dom $\mathcal{G}_1 = \mathcal{D}_1$, triggers a switching event of the logic variable, and the map

$$\mathcal{G}_2(\mathbf{x}) := \left\{ \begin{bmatrix} \mathbf{x}_0 \\ T(\mathbf{r}, \mathbf{z}, \mathbf{r}_3) \\ \check{\boldsymbol{\omega}}\left(\mathbf{x}_0, \mathbf{p}_d^{(3)}\right) \end{bmatrix} : \mathbf{p}_d^{(3)} \in r\overline{\mathbb{B}} \right\}, \tag{25}$$

where dom $\mathcal{G}_2 = \mathcal{D}_2$, triggers a sampling event. We now state the main result on stability of a zero tracking error set for $\mathcal{H}$, whose proof is referred to Appendix F.

Theorem 1. *Suppose Assumption 1 holds, then the set* $\mathcal{A} := \left\{ \mathbf{x} \in \mathcal{S}_{\mathbf{x}} : \mathbf{z} = \mathbf{0}, \mathbf{r}_3 = q\frac{g\mathbf{e}_3 - \ddot{\mathbf{p}}_d}{|g\mathbf{e}_3 - \ddot{\mathbf{p}}_d|} \right\}$ *is globally asymptotically stable for the hybrid system* $\mathcal{H}$ *defined by (23).*

Remark 2. The convergence of error state $\mathbf{z}$ to the origin corresponds to trajectory tracking, while the convergence of $\mathbf{r}_3$ corresponds to the fact that the thrust direction tends to align itself with the desired one, which solves the problem defined in **Problem Statement**.

4.4 | Avoidance of Zeno solutions for the controller in Section 4.3

To have a positive lower bound on the inter-event time, which implies the absence of Zeno behavior of solutions, is essential for practical implementation of the proposed controller on digital platforms, and the following corollary provides a method that ensures absence of Zeno solutions by modifying $\mathcal{H}$. Notice that for the controller in Section 4.2, $\mathcal{G}_0(\mathcal{D}_0) \subset \mathcal{C}_0 \setminus \mathcal{D}_0$, which implies that $\mathcal{G}_0(\mathcal{D}_0) \cap \mathcal{D}_0 = \emptyset$, which implies the existence of some positive lower bound between consecutive jumps for each maximal solution to $\mathcal{H}_0$ by lemma 2.7 in the work of Sanfelice et al.[34] For the controller in Section 4.3, multiple jumps are possible at the same flow time. In fact, because the set $\mathcal{G}^k(\mathcal{D}) \cap \mathcal{D} \neq \emptyset$ is nonempty for each $k \in \mathbb{Z}_{>0}$ with $\mathcal{G}^k$ given in Definition 2, there exists a complete discrete solution at $\mathcal{A}$, for example, $\mathbf{x}(0, j+1) = \mathcal{G}_2(\mathbf{x}(0, j))$ such that the solution $\mathbf{x}(0, j) \in \mathcal{A}$ for each $j \in \mathbb{Z}_{\geq 0}$. A straightforward fix for this problem is to remove the possibility of any jumps within an arbitrarily small neighborhood $\mathcal{A}$, inspired by the work of Postoyan et al.[16] and formalized in the following corollary, whose proof is given in Appendix G.

Corollary 1. *Suppose Assumption 1 holds. Let* $\widehat{\mathcal{A}} := \{\mathbf{x} \in \mathcal{S}_{\mathbf{x}} : \widetilde{V}_q(\mathbf{x}) \leq \delta\}$ *with some* $\delta \in \mathbb{R}_{>0}$ *and consider the hybrid system*

$$\widehat{\mathcal{H}} := (\mathcal{F}, \widehat{\mathcal{C}}_1 \cap \widehat{\mathcal{C}}_2, \widehat{\mathcal{G}}, \widehat{\mathcal{D}}_1 \cup \widehat{\mathcal{D}}_2), \tag{26}$$

where $\widehat{\mathcal{C}}_1 := \mathcal{C}_1 \cup \widehat{\mathcal{A}}$, $\widehat{\mathcal{C}}_2 := \mathcal{C}_2 \cup \widehat{\mathcal{A}}$, $\widehat{\mathcal{D}}_1 := \mathcal{D}_1 \cap \overline{\mathcal{S}_{\mathbf{x}} \setminus \widehat{\mathcal{A}}}$, $\widehat{\mathcal{D}}_2 := \mathcal{D}_2 \cap \overline{\mathcal{S}_{\mathbf{x}} \setminus \widehat{\mathcal{A}}}$, $\widehat{\mathcal{G}}(\mathbf{x}) := \mathcal{G}_1(\mathbf{x}) \cup \mathcal{G}_2(\mathbf{x})$ *for each* $\mathbf{x} \in \widehat{\mathcal{D}}_1 \cup \widehat{\mathcal{D}}_2$, *and* $\mathcal{F}$, $\mathcal{C}_1$, $\mathcal{C}_2$, $\mathcal{G}_1$, $\mathcal{G}_2$, $\mathcal{D}_1$, *and* $\mathcal{D}_2$ *are given in Section 4.3. Then, the set* $\widehat{\mathcal{A}}$ *is globally asymptotically stable for the hybrid system* $\widehat{\mathcal{H}}$ *and* $\widehat{\mathcal{H}}$ *has no Zeno solutions.*

Remark 3. We notice the trade-off between achieving global asymptotic stabilization and avoidance of Zeno solutions. For practical consideration, we can choose δ arbitrarily small to meet our tolerance of arbitrary small errors in trajectory tracking.

5 | SIMULATION RESULTS

In order to verify the performance of the proposed control scheme, this section presents simulation results by making use of MATLAB/Simulink software with the hybrid equation solver.[35]

A circle parameterized in flow time is chosen to be the position reference trajectory defined as $\mathbf{p}_d(t) = \left(\frac{6}{5}\cos(t), \frac{6}{5}\sin(t), -0.5\right)$ m for each $t \in \mathbb{R}_{\geq 0}$, such that Assumption 1 holds. For each $i \in \{1, 2, 3\}$, the β_i function in (9) is chosen as $\beta_i(\xi) = \frac{2K_{\beta_i}}{\pi}\arctan\left(\frac{\pi M_{\beta_i}}{2K_{\beta_i}}\xi\right)$ for each $\xi \in \mathbb{R}$, where $M_{\beta_i}, K_{\beta_i} \in \mathbb{R}_{>0}$. In each subsequent simulation, the initial states are chosen in $\mathcal{S}_{\mathbf{x}}$ and the hybrid systems are simulated for a maximum of 20 s and 3500 times. Parameters used in

subsequent simulations are $m = 0.2$ kg, $g = 9.8$ m s^{-2}, $k_{\mathbf{p}} = 2$, $k_{\mathbf{v}} = 2$, $\gamma = 0.8$, $k_{\omega} = 5$, $M_{\beta} = (1,1,1)$, $K_{\beta} = (1,1,1)$, $\epsilon = 20$, and $\eta = 36$, such that the inequality (10) holds.

5.1 | Simulation results of the controller in Section 4.3

We choose *the sampling tuning factor* as $\sigma = 0.9$ and the initial state is chosen such that

$$\mathbf{x}(0,0) \in C \cap D_1, \tag{27}$$

wherein

$$\mathbf{z}_1(0,0) \approx (-4.2409, -1.9158, -1.2518)\ m,\ \mathbf{z}_2(0,0) \approx (0.4980, 0.3075, -0.4955)\ \text{m s}^{-1},$$
$$\mathbf{r}_3(0,0) \approx (0.4058, 0.1505, -0.9015),\ q(0,0) = 1,\ s_1(0,0) = 0\ N,\ \mathbf{s}_2(0,0) = \mathbf{0}\ \text{s}^{-1}.$$

Two possible solutions to the hybrid system $\mathcal{H}$ defined in Section 4.3 with the same initial state are shown in Figure 3, denoted by $\mathbf{x}$ (cross markers) and $\mathbf{x}^*$ (circle markers). The solution $\mathbf{x}$ undergoes one switching for the value of q, that is, $q(t,j) = -1$ for each $(t,j) \in \text{dom}\ \mathbf{x} \setminus \{(0,0)\}$, while the solution $\mathbf{x}^*$ undergoes no switching for the value of q^*, that is, $q^*(t,j) = 1$ for each $(t,j) \in \text{dom}\ \mathbf{x}^*$. Despite the difference in the time evolution of these two solutions, they both approach the set $\mathcal{A}$. However, the solution $\mathbf{x}$ converges to $\mathcal{A}$ faster than $\mathbf{x}^*$ due to a smaller initial angular distance with respect to the set $\mathcal{A}$. $\mathbf{x}$ represents the case when the vehicle performs trajectory tracking in inverted flight, that is, $s_1(t,j) \leq 0$ for each $(t,j) \in \text{dom}\ \mathbf{x}$. On the other hand, the solution $\mathbf{x}^*$ manifests a thrust direction reversal for the vehicle at $t \approx 0.32$ s, witnessed by a surge of $|\mathbf{s}_2^*|$, and eventually achieves trajectory tracking in upright flight. It is interesting to note that the proposed controller reacts against increasing error norms by increasing number of jumps (which are samples of actuation signals rather than the switching of logic variables). Nevertheless, the inter-event time between consecutive jumps becomes shorter when both solutions approach the set $\mathcal{A}$, implying possible Zeno behavior, as shown in Figure 3(D). Note that we are simulating for a maximum of 20 s and 3500 times. If we raise these limits, then the hybrid domains of both $\mathbf{x}$ and $\mathbf{x}^*$ in Figure 3(D) will be extended.

Remark 4. If we choose the position reference trajectory to be a fixed point in space, then there may not be accumulating events when approaching the zero tracking error set $\mathcal{A}$. This is due to the fact that position reference trajectories with constant acceleration, in the form of $\mathbf{p}_d(t) = \mathbf{a}t^2 + \mathbf{b}t + \mathbf{c}$ for each $t \in \mathbb{R}_{\geq 0}$ with $\mathbf{a}, \mathbf{b}, \mathbf{c} \in \mathbb{R}^3$, may result in continuous solution without jumps within $\mathcal{A}$ and therefore frequent sampling is not needed. To reflect Zeno solutions that are mentioned in Section 4.4, we decided to choose a circle to be the position reference trajectory.

5.2 | Simulation results of the controller in Section 4.4

We choose *the sampling tuning factor* as $\sigma = 0.9$ and choose $\delta = 10^{-3}$ for the set $\widehat{\mathcal{A}}$ that we would like to stabilize. The initial state and other parameters are chosen to be the same as those in Section 5.1. Two possible solutions to the hybrid system $\widehat{\mathcal{H}}$ defined in Section 4.4 with the same initial state are shown in Figure 3, denoted by $\widehat{\mathbf{x}}$ (square markers) and $\widehat{\mathbf{x}}^*$ (diamond markers). Similar to Section 5.1, the solution $\widehat{\mathbf{x}}$ undergoes one switching for the value of q, that is, $\widehat{q}(t,j) = -1$ for each $(t,j) \in \text{dom}\ \widehat{\mathbf{x}} \setminus \{(0,0)\}$, while the solution $\widehat{\mathbf{x}}^*$ undergoes no switching for the value of $\widehat{q}^*$, that is, $\widehat{q}^*(t,j) = 1$ for each $(t,j) \in \text{dom}\ \widehat{\mathbf{x}}^*$. In Figure 3(D), the dotted lines represent the time when the solutions $\widehat{\mathbf{x}}$ and $\widehat{\mathbf{x}}^*$ reach the set $\widehat{\mathcal{A}}$ at around 6.36 and 12.25 s, respectively. Before reaching $\widehat{\mathcal{A}}$, the jumps of $\widehat{\mathbf{x}}$ (or $\widehat{\mathbf{x}}^*$) of Section 5.2agree with those of $\mathbf{x}$ (or $\mathbf{x}^*$) of Section 5.1. After reaching $\widehat{\mathcal{A}}$, the jumps of $\widehat{\mathbf{x}}$ (or $\widehat{\mathbf{x}}^*$) versus time manifest an almost periodic pattern, whereas the update frequency of $\mathbf{x}$ (or $\mathbf{x}^*$) tends to increase. Nonetheless, the error norms of $\widehat{\mathbf{x}}$ (or $\widehat{\mathbf{x}}^*$) stay close to those of $\mathbf{x}$ (or $\mathbf{x}^*$), as witnessed in Figure 3(A),(B). In fact, how close depends on the chosen parameter δ, as we will study in the sequel.

Next, we explore the impact of *the sampling tuning factor* on the controller performance by varying σ. We choose the initial state $\mathbf{x}_\sigma(0,0)$ such that

$$\mathbf{z}_{1,\sigma(0,0)} = (10,10,10)\ \text{m},\ \mathbf{z}_{2,\sigma(0,0)} = (10,10,10)\ \text{m s}^{-1},\ \mathbf{r}_{3\sigma}(0,0) = \mathbf{e}_3,\ q_\sigma(0,0) = 1,\ s_{1,\sigma}(0,0) = 0\ N,\ \mathbf{s}_{2,\sigma}(0,0) = \mathbf{0}\ s^{-1}.$$

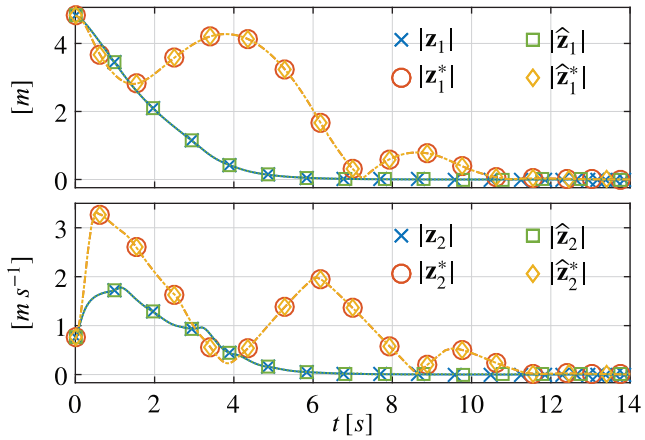

(A) Time evolution of the norms of position errors and velocity errors.

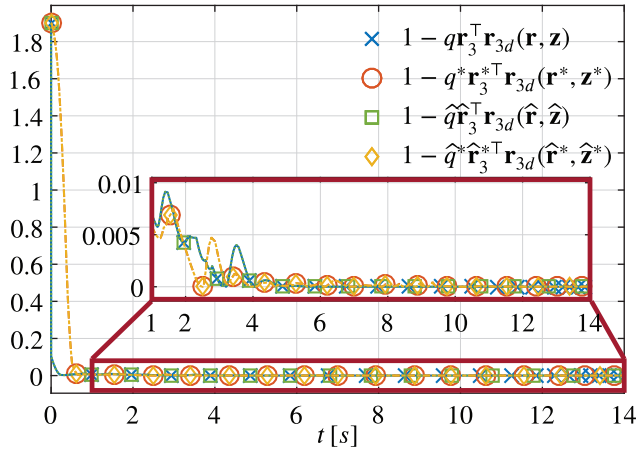

(B) Time evolution, in split windows, of the angular distances.

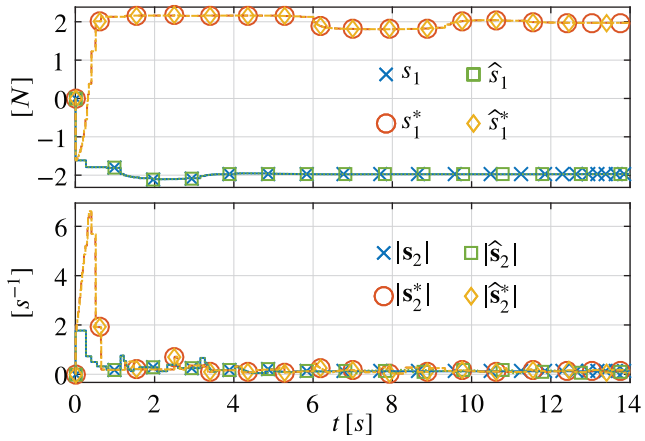

(C) Time evolution of the sampled thrusts and the sampled angular velocity norms.

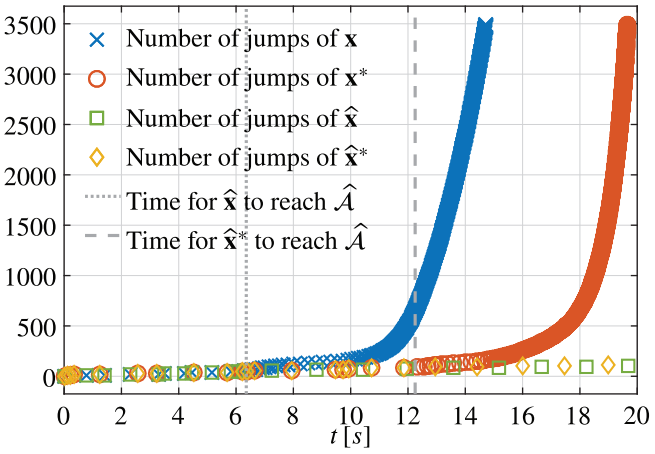

(D) Number of jumps against time.

FIGURE 3 Simulation results of time evolution of two possible solutions $\mathbf{x}$ (inverted flight) and $\mathbf{x}^*$ (upright flight) to $\mathcal{H}$ in (23) and two possible solutions $\hat{\mathbf{x}}$ (inverted flight) and $\hat{\mathbf{x}}^*$ (upright flight) to $\hat{\mathcal{H}}$ in (26), all starting from the initial state $\mathbf{x}(0,0)$ in (27). (A) Time evolution of the norms of position errors and velocity errors; (B) Time evolution, in split windows, of the angular distances; (C) Time evolution of the sampled thrusts and the sampled angular velocity norms; (D) Number of jumps against time

Samples of *the sampling tuning factor* σ are drawn from the interval $]0,1[\subset\mathbb{R}$ to study the impact of σ on the control performance associated with each corresponding solution $\mathbf{x}_\sigma$, summarized in Table 1. As the value of σ increases, $T_{\hat{\mathcal{A}}}$ tends to decrease while $J_{\hat{\mathcal{A}}}$ tends to increase. Also, it is interesting to notice the trade-off between faster convergence and smaller average inter-event time, which agrees with our expectation that the event-triggered controller behaves more like a continuous time controller as σ approaches 1.

We also explore the impact of δ on the control performance as discussed in Remark 3. The initial state $\mathbf{x}_\delta(0,0)$ is chosen to equal $\mathbf{x}_\sigma(0,0)$, *the sampling tuning factor* $\sigma = 0.9$, and samples of δ are selected from $\mathbb{R}_{>0}$ to study its impact on the control performance associated with each corresponding solution $\mathbf{x}_\delta$, summarized in Table 2. The analysis in Appendices F and G suggests an upper bound for the steady state trajectory tracking error be $\alpha_1^{-1}(\delta)$ for some function α_1 of class $\mathcal{K}_\infty$, which increases with larger δ. With larger δ, both the time and triggers it takes to reach $\hat{\mathcal{A}}$ decrease, and the RMS values of the steady state errors in norm (trajectory tracking error $|\mathbf{x}_\delta|_{\mathcal{A}}$, position error $|\mathbf{z}_{1\delta}|$, linear velocity error $|\mathbf{z}_{2\delta}|$, angular velocity error $|\mathbf{z}_{3\delta}|$) tend to increase. Therefore, we can reduce the upper bound for the steady-state trajectory tracking error by picking smaller δ, but at the expense of longer time and more triggers before reaching $\hat{\mathcal{A}}$.

A separate simulation is done to compare the performance the controller with that of a controller with periodic sampling, see Appendix H for detail.

TABLE 1 Controller performance for different σ

σ (s^{-1})	$T_{\widehat{\mathcal{A}}}$ $(s)^a$	$J^b_{\widehat{\mathcal{A}}}$	$\overline{\Delta}_T$ $(s)^c$
0.1	70.41	288	0.24
0.3	62.35	262	0.24
0.5	57.23	271	0.21
0.7	57.78	391	0.15
0.9	49.11	716	0.069

[a]Time it takes for $\mathbf{x}_\sigma$ to reach $\widehat{\mathcal{A}}$.
[b]Number of triggers it takes for $\mathbf{x}_\sigma$ to reach $\widehat{\mathcal{A}}$.
[c]Average inter-event time in the time interval $[0, T_{\widehat{\mathcal{A}}}]$.

TABLE 2 Controller performance for different δ

$\delta \times 10^{-4}$	$T_{\widehat{\mathcal{A}}}$ $(s)^a$	$J^b_{\widehat{\mathcal{A}}}$	$\lvert\mathbf{x}_\delta\rvert^c_{\mathcal{A}}$	$\lvert\mathbf{z}_{1\delta}\rvert^c$	$\lvert\mathbf{z}_{2\delta}\rvert^c$	$\lvert\mathbf{z}_{3\delta}\rvert^{c,d}$
5	49.82	730	0.0070	0.0024	0.0052	0.0029
10	49.11	716	0.0090	0.0023	0.0065	0.0041
50	48.41	698	0.0183	0.0027	0.0124	0.0047
100	48.30	697	0.0257	0.0041	0.0173	0.0132
500	48.14	696	0.0585	0.0168	0.0378	0.0293

[a]Time it takes for $\mathbf{x}_\delta$ to reach $\widehat{\mathcal{A}}$.
[b]Number of triggers it takes for $\mathbf{x}_\delta$ to reach $\widehat{\mathcal{A}}$.
[c]RMS of steady state value.
[d]$\lvert\mathbf{z}_{3\delta}\rvert := \lvert\mathbf{r}_{3\delta} - q_\delta \mathbf{r}_{3d}(\mathbf{r}_\delta, \mathbf{z}_\delta)\rvert$.

6 | EXPERIMENTAL RESULTS

The rapid prototyping and testing setup at the SCORE laboratory,[36] University of Macau, was used to experimentally validate our algorithm. Experiments were conducted in a MATLAB/Simulink environment that integrated an optical motion capture system,[37] and radio communication with the quadrotor. The quadrotor used for the experiments is a radio-controlled BLADE 200QX.[38] The vehicle has a flying weight of 0.216 kg (batteries, radio receiver, and motion capture markers included). It has four brushless motors which drive four propellers located at the end of each arm. The experimental quadrotor lacks on-board sensors and the state of the quadrotor must be estimated resorting to external sensors. To this effect, we placed six motion capture markers with which the position and orientation information can be obtained through the motion capture system. The linear velocity of the quadrotor can be estimated from the position measurements by a simple backward Euler difference, with relatively high accuracy and low noise level. The state measurements from the motion capture system are obtained every 0.01 s while the actuation signals are sent through the radio frequency transmitter every 0.045 s.

A graphical representation of the overall architecture is shown in Figure 4. We use three computer systems: one running the motion capture software; a second one generating the computed actuation signals to be sent to the third computer through Ethernet; the third one receiving the computed actuation signals and sending them through serial port to the RF module. This configuration is to avoid jitter in the transmission of the serial port signals to the RF module when running all the systems in the same computer, which can lead to erratic communication with the quadrotor.

6.1 | Fixed-point tracking

In fixed-point tracking, the reference trajectory $\mathbf{p}_d(t) = (0, 0, -0.5)\,\mathrm{m}$ for each $t \in \mathbb{R}_{\geq 0}$. The controller parameters are the same as those of Section 5 except for $m = 0.216$ kg, $g = 9.79\,\mathrm{m\,s^{-2}}$, $K_\beta = (1, 1, 4.3)$, $\sigma = 0.9$, and $\delta = 10^{-3}$. We tested the tracking performance of the quadrotor in two scenarios: inverted flight and upright flight. For the former case, we held it steady above the ground in order not to crash the quadrotor and release it at $t = 0$ s, a video clip available online to

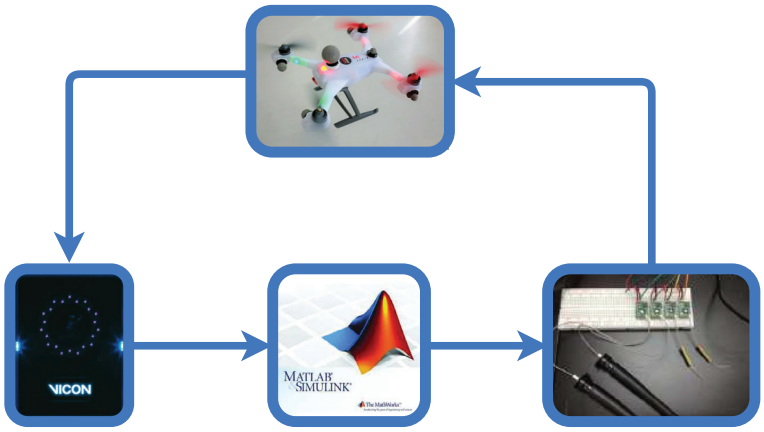

FIGURE 4 Quadcopter integrated measurement and command architecture

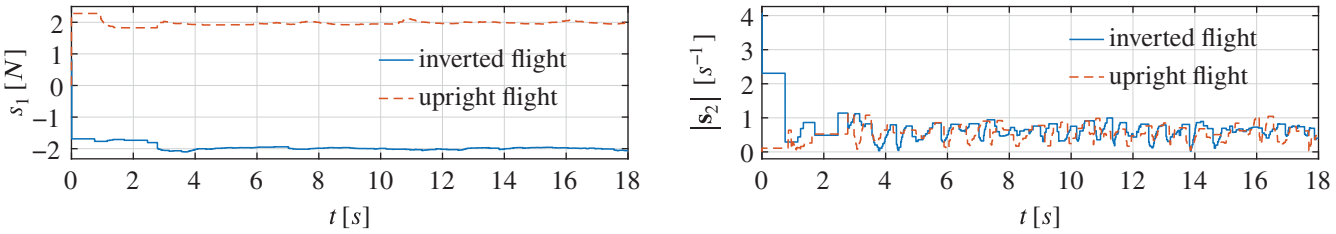

FIGURE 5 Experimental results of time evolution of two possible solutions $\mathbf{x}$ (inverted flight) and $\mathbf{x}^*$ (upright flight) to $\widehat{\mathcal{H}}$ in (26) for fixed-point tracking

capture the behavior of the flying quadrotor.[39] For the latter case, we placed the quadrotor on the ground and made the event-triggered controller work from $t = 0$ s.

Time evolution of the sampled actuation signals, depicted in Figure 5, demonstrate sampling pattern resulting from the event-triggered controller. Due to the hysteresis effect of actuation signals, the quadrotor underwent a thrust surge and an angular velocity surge at $t = 0$ s for the inverted flight. Given the sampling frequency of 100 Hz of our experimental setup, we obtain the following inter-event data: for upright flight, the median and maximum times between events are 0.05 and 1.16 s, respectively; for inverted flight, the median and maximum times between events are 0.04 and 0.75 s, respectively. These results demonstrate that event-triggered control enables a significant reduction of the number of updates without compromising the stability of the closed-loop system.

For the tracking performance of the thrust direction vector $\mathbf{r}_3$ shown in Figure 6, the angular errors $1 - q\mathbf{r}_3\mathbf{r}_{3d}(\mathbf{r}, \mathbf{z})$ stay closely to 0 for both scenarios after the initial transients. Position tracking performance was illustrated in Figure 7. The position vector first went through initial transients, then stayed within a neighborhood of the reference position vector. Reasons for its deviations from the reference position vector are manifold. First, there are unmodeled dynamics of the quadrotor model, for example, inner control loop that is assumed to response sufficiently fast. Second, we ignore possible noise additive to the state measurement from VICON and to the quadrotor during flight. Third, state measurement of the quadrotor is itself a sampled data from the actual state. Lastly, the mass may vary for each replacement of the internal battery and the parameter $g = 9.79\ \mathrm{m\,s^{-2}}$ may be different from the actual local gravity, which induce a steady-state error that is prominent in the z-component of the position vector, witnessed by the last subfigure of Figure 7. This is due to the fact that we are using a proportional feedback law in stabilizing the position and linear velocity dynamics, see (8).

6.2 | Circular trajectory tracking

The reference trajectory is a circle in the space, that is, $\mathbf{p}_d(t) = \left(\frac{6}{5}\cos(t), \frac{6}{5}\sin(t), -0.5\right)$ m for each $t \in \mathbb{R}_{\geq 0}$, and we decrease the z-component of K_β such that $K_\beta = (1, 1, 1)$. We only show the position tracking performance of upright flight for simplicity. It is witnessed in Figure 8 that the quadrotor follows the position reference closely within 0.1 m along the (x, y)-component after the initial transient, while the steady-state position error of the z-component gets a little bit worse

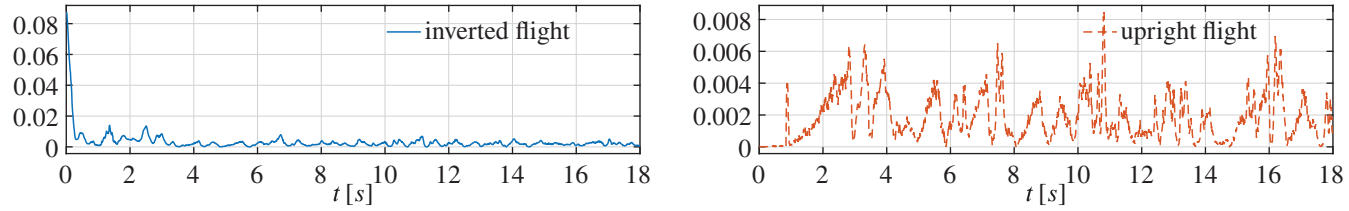

FIGURE 6 Comparison of the angular errors between inverted flight and upright flight for fixed-point tracking

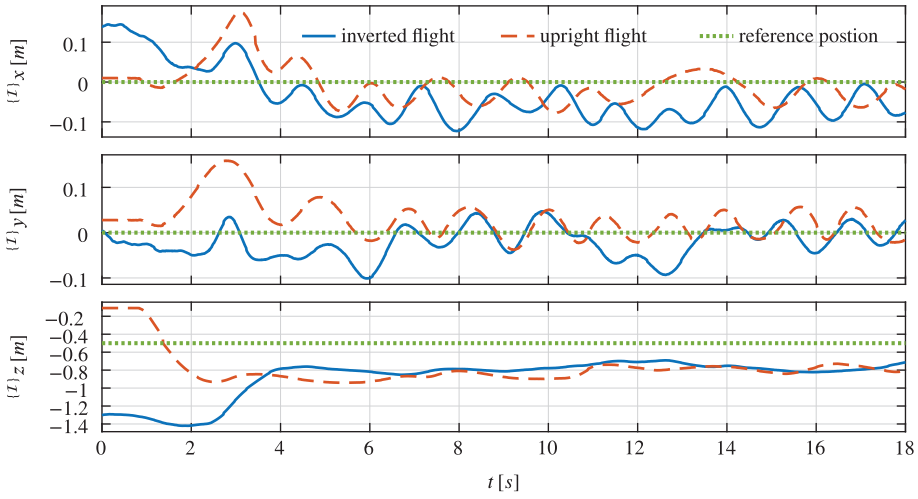

FIGURE 7 Comparison of the tracking performance of the position components in the inertial frame $\{\mathcal{I}\}$ between inverted flight and upright flight for circular trajectory tracking

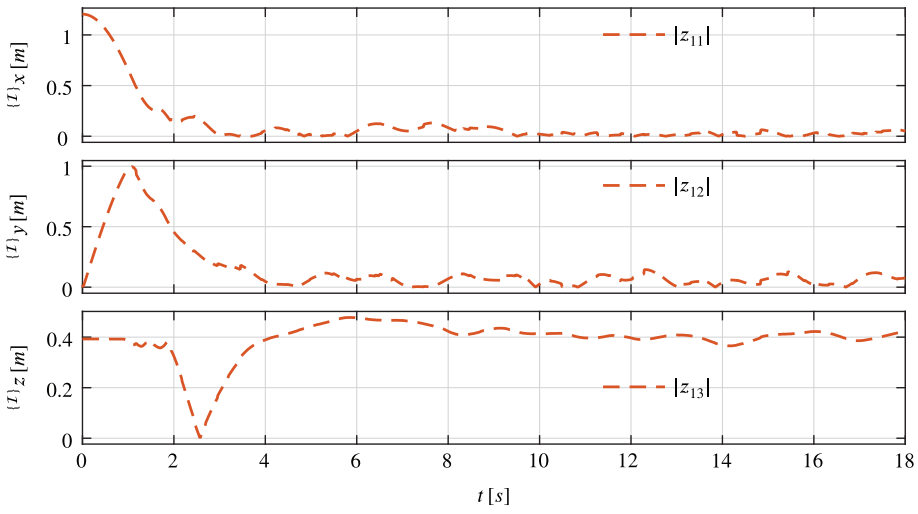

FIGURE 8 Absolute values of position error components (z_{11}, z_{12}, z_{13}): $= \mathbf{z}_1$ in the inertial frame $\{\mathcal{I}\}$ of upright flight for circular trajectory tracking

than that of fixed-point tracking in Section 6.1, largely due to the decrease of the gain K_{β_3}. The average inter-event time is 0.068 s, with a minimum inter-event time of 0.01 s and a maximum of 0.61 s. The median inter-event time is 0.04 s.

7 | CONCLUSION

This paper presented a solution to the problem of trajectory tracking for a class of underactuated quadrotors, taking into consideration the sampling of the actuation signals using zero-order-hold devices. Based on the hybrid dynamical model of the system, an event-triggered control law was devised such that the zero tracking error set is rendered globally asymptotically stable for the closed-loop hybrid system. For practical implementation, we modified the data of the hybrid

system in order to avoid Zeno solutions. Both simulations and experiments were conducted, validating the performance of our controller.

ACKNOWLEDGEMENTS

This work was supported by the Macao Science and Technology Development Fund under Grant FDCT/0031/2020/AFJ, by the University of Macau, Macao, China, under Project MYRG2018- 00198-FST, by the Fundação para a Ciência e a Tecnologia (FCT) through LARSyS - FCT Project UIDB/50009/2020 and LAETA - FCT Project UIDB/50022/2020, and by FCT Scientific Employment Stimulus grant CEECIND/04652/2017.

DATA AVAILABILITY STATEMENT

The data that support the findings of this study are available from the corresponding author upon reasonable request.

ORCID


Xuan-Zhi Zhu https://orcid.org/0000-0002-5970-7508

REFERENCES

1. Hoffmann GM, Wasl SL, Tomlin CJ. Quadrotor helicopter trajectory tracking control. Paper presented at: Proceedings of the AIAA Guidance, Navigation, and Control Conference, Honolulu, HI, USA; 2012.
2. Koo TJ, Sastry S. Output tracking control design of a helicopter model based on approximate linearization. Paper presented at: Proceedings of the 37th IEEE Conference on Decision and Control (Cat. No.98CH36171), Tampa, FL, USA; Vol. 4, 1998:3635-3640.
3. Xu R, Ozguner U. Sliding mode control of a quadrotor helicopter. Paper presented at: Proceedings of the 45th IEEE Conference on Decision and Control, San Diego, CA, USA; 2006:4957-4962.
4. Cabecinhas D, Cunha R, Silvestre C. A nonlinear quadrotor trajectory tracking controller with disturbance rejection. *Control Eng Pract*. 2014;26:1-10.
5. Dydek ZT, Annaswamy AM, Lavretsky E. Adaptive control of quadrotor UAVs: a design trade study with flight evaluations. *IEEE Trans Control Syst Technol*. 2013;21(4):1400-1406. https://doi.org/10.1109/TCST.2012.2200104.
6. Casau P, Sanfelice RG, Cunha R, Silvestre C. A globally asymptotically stabilizing trajectory tracking controller for fully actuated rigid bodies using landmark-based information. *Int J Robust Nonlinear Control*. 2015;25(18):3617-3640. https://doi.org/10.1002/rnc.3283.
7. Åström KJ, Bernhardsson B. Comparison of periodic and event based sampling for first-order stochastic systems. *IFAC Proc Vol*. 1999;32(2):5006-5011.
8. Åarzén K-E. A simple event-based PID controller. *IFAC Proc Vol*. 1999;32(2):8687-8692.
9. Otanez PG, Moyne JR, Tilbury DM. Using deadbands to reduce communication in networked control systems. Paper presented at: Proceedings of the 2002 American Control Conference (IEEE Cat. No.CH37301), Anchorage, AK, USA, Vol.4; 2002:3015-3020.
10. Kofman E, Braslavsky JH. Level crossing sampling in feedback stabilization under data-rate constraints. Paper presented at: Proceedings of the 45th IEEE Conference on Decision and Control, San Diego, CA, USA; 2006:4423-4428.
11. Tabuada P. Event-triggered real-time scheduling of stabilizing control tasks. *IEEE Trans Automat Contr*. 2007;52(9):1680-1685. https://doi.org/10.1109/TAC.2007.904277.
12. Seuret A, Prieur C, Marchand N. Stability of non-linear systems by means of event-triggered sampling algorithms. *IMA J Math Control Inf*. 2014;31(3):415-433. https://doi.org/10.1093/imamci/dnt018.
13. Abdelrahim M, Postoyan R, Daafouz J, Nešić D. Stabilization of nonlinear systems using event-triggered output feedback controllers. *IEEE Trans Automat Contr*. 2016;61(9):2682-2687. https://doi.org/10.1109/TAC.2015.2502145.
14. Nešić D, Teel AR, Carnevale D. Explicit computation of the sampling period in emulation of controllers for nonlinear sampled-data systems. *IEEE Trans Autom Control*. 2009;54(3):619-624. https://doi.org/10.1109/TAC.2008.2009597.
15. Heemels WPMH, Sandee JH, Van Bosch PPJ. Analysis of event-driven controllers for linear systems. *Int J Control*. 2008;81(4):571-590. https://doi.org/10.1080/00207170701506919.
16. Postoyan R, Tabuada P, Nešić D, Anta A. A framework for the event-triggered stabilization of nonlinear systems. *IEEE Trans Automat Contr*. 2015;60(4):982-996. https://doi.org/10.1109/TAC.2014.2363603.
17. Yu H, Fei H. A Lyapunov-based small-gain approach on design of triggering conditions in event-triggered control systems. *Int J Robust Nonlinear Control*. 2016;26(13):2938-2960. https://doi.org/10.1002/rnc.3488.
18. Postoyan R, Bragagnolo MC, Galbrun E, Daafouz J, Nešić D, Castelan E. Nonlinear event-triggered tracking control of a mobile robot: design, analysis and experimental results. Paper presented at: Proceedings of the 9th IFAC Symposium on Nonlinear Control Systems, NOLCOS; 2013:318-323; Toulouse, France.
19. Téllez-Guzmán JJ, Guerrero CF, Durand S, Marchand N, Lucio-Maya R. Event-based LQR control for attitude stabilization of a quadrotor. Paper presented at: Proceedings of the 15th IFAC Latinamerican Control Conference (CLCA'12); 2012; Lima, Peru.
20. Marchand N, Durand S, Castellanos JFG. A general formula for event-based stabilization of nonlinear systems. *IEEE Trans Automat Contr*. 2013;58(5):1332-1337. https://doi.org/10.1109/TAC.2012.2225493.
21. Guerrero-Castellanos J-F, Téllez-Guzmán JJ, Durand S, Marchand N, Alvarez-Muñoz JU, Gonzalez-Diaz VR. Attitude stabilization of a quadrotor by means of event-triggered nonlinear control. *J Intell Robot Syst*. 2014;73(1-4):123-135.

22. Guerrero-Castellanos JF, Marchand N, Durand S, Vega-Alonzo A, Téllez-Guzmán JJ. Event-triggered attitude control for flying robots using an event approach based on the control. Paper presented at: Proceedings of the 2015 International Conference on Event-based Control, Communication, and Signal Processing (EBCCSP), Krakow, Poland; 2015:1-8.
23. Yu P, Ding L, Liu Z-W, Guan Z-H. Leader-follower flocking based on distributed event-triggered hybrid control. *Int J Robust Nonlinear Control*. 2016;26(1):143-153. https://doi.org/10.1002/rnc.3308.
24. Durand S, Boisseau B, Marchand N, Guerrero-Castellanos JF. Event-based PID control application to a mini quadrotor helicopter. *J Control Eng Appl Inform*. 2018;20(1):36-47.
25. Cuenca Á, Antunes DJ, Castillo A, García P, Khashooei BA, Heemels WPMH. Periodic event-triggered sampling and dual-rate control for a wireless networked control system with applications to UAVs. *IEEE Trans Ind Electron*. 2019;66(4):3157-3166.
26. Bhat SP, Bernstein DS. A topological obstruction to continuous global stabilization of rotational motion and the unwinding phenomenon. *Syst Control Lett*. 2000;39(1):63-70. https://doi.org/10.1016/S0167-6911(99)00090-0.
27. Mayhew CG, Teel AR. Global stabilization of spherical orientation by synergistic hybrid feedback with application to reduced-attitude tracking for rigid bodies. *Automatica*. 2013;49(7):1945-1957.
28. Michini B, Redding J, Kemal UN, Cutler M, How JP. Design and flight testing of an autonomous variable-pitch quadrotor. Paper presented at: Proceedings of the 2011 IEEE International Conference on Robotics and Automation, Shanghai, China; 2011:2978-2979.
29. Cutler M, Ure NK, Michini B, How J. Comparison of fixed and variable pitch actuators for agile quadrotors. Paper presented at: Proceedings of the AIAA Guidance, Navigation, and Control Conference, Portland, OR, USA; 2011.
30. Goebel R, Sanfelice RG, Teel AR. *Hybrid Dynamical Systems: Modeling, Stability, and Robustness*. Princeton, NJ: Princeton University Press; 2012.
31. Craig JJ. *Introduction to Robotics: Mechanics and Control*. Upper Saddle River, NJ: Pearson/Prentice Hall; 2005.
32. Casau P, Sanfelice RG, Cunha R, Cabecinhas D, Silvestre C. Robust global trajectory tracking for a class of underactuated vehicles. *Automatica*. 2015;58:90-98. https://doi.org/10.1016/j.automatica.2015.05.011.
33. Khalil HK. *Nonlinear Systems*. Upper Saddle River, NJ: Prentice Hall; 2002.
34. Sanfelice RG, Goebel R, Teel AR. Invariance principles for hybrid systems with connections to detectability and asymptotic stability. *IEEE Trans Automat Contr*. 2007;52(12):2282-2297. https://doi.org/10.1109/TAC.2007.910684.
35. Sanfelice RG, Copp DA, Pablo N. Hybrid equations (HyEQ) toolbox v2.02 a toolbox for simulating hybrid systems in MATLAB/Simulink; https://hybrid.soe.ucsc.edu/software/.
36. Sensor based Cooperative Robotics Research (SCORE) laboratory, at the Department of Electrical and Computer Engineering of the Faculty of Science and Technology, University of Macau; 2018. https://score.fst.um.edu.mo/.
37. Vicon Motion Systems Ltd; 2018. https://www.vicon.com/.
38. Horizon Hobby Inc; 2014. http://www.bladehelis.com/.
39. Event-triggered control for trajectory tracking of a quadrotor vehicle; 2019. https://youtu.be/eD8iBOllcmU/.
40. Sundaram RK. *A First Course in Optimization Theory*. New York, NY, USA: Cambridge University Press; 1996.

How to cite this article: Zhu X-Z, Casau P, Silvestre C. Event-triggered global trajectory tracking control of a quadrotor: Synthesis, simulations, and experiments. *Int J Robust Nonlinear Control*. 2021;31:6144–6165. https://doi.org/10.1002/rnc.5565

APPENDIX A

Proof of Lemma 1. We first examine outer semicontinuity of $\mathcal{M}$. By lemma 5.10 in the work of Goebel et al.,[30] the set $\mathcal{S}_1 := \{(\mathbf{x},\mathbf{y}) \in \mathbb{R}^n \times \mathbb{R}^n : \mathbf{x} \in \mathcal{A}_1, \mathbf{y} \in \mathcal{M}_1(\mathbf{x})\}$ is closed relative to $\mathcal{A}_1 \times \mathbb{R}^n$ and the set $\mathcal{S}_2 := \{(\mathbf{x},\mathbf{y}) \in \mathbb{R}^n \times \mathbb{R}^n : \mathbf{x} \in \mathcal{A}_2, \mathbf{y} \in \mathcal{M}_2(\mathbf{x})\}$ is closed relative to $\mathcal{A}_2 \times \mathbb{R}^n$. Let $\mathcal{S} := \{(\mathbf{x},\mathbf{y}) \in \mathbb{R}^n \times \mathbb{R}^n : \mathbf{x} \in \mathcal{A}_1 \cup \mathcal{A}_2, \mathbf{y} \in \mathcal{M}(\mathbf{x})\}$, then it follows from the construction of the set-valued mapping $\mathcal{M}$ that $\mathcal{S} = \mathcal{S}_1 \cup \mathcal{S}_2$. By the assumption that both $\mathcal{A}_1$ and $\mathcal{A}_2$ are closed relative to $\mathbb{R}^n$, we have that both $\mathcal{S}_1$ and $\mathcal{S}_2$ are closed relative to $\mathbb{R}^n \times \mathbb{R}^n$. It follows that $\mathcal{S}$ is closed relative to $\mathbb{R}^n \times \mathbb{R}^n$. Furthermore, $(\mathcal{A}_1 \cup \mathcal{A}_2) \times \mathbb{R}^n$ is closed relative to $\mathbb{R}^n \times \mathbb{R}^n$, which implies that $\mathcal{S}$ is closed relative to $(\mathcal{A}_1 \cup \mathcal{A}_2) \times \mathbb{R}^n$. Therefore, $\mathcal{M}$ is outer semicontinuous relative to $\mathcal{A}_1 \cup \mathcal{A}_2$. Next, we examine local boundedness of $\mathcal{M}$. For each $\mathbf{x} \in \mathcal{A}_1 \setminus \mathcal{A}_2$, there exists $\delta_1 \in \mathbb{R}_{>0}$ and $\epsilon_1 \in \mathbb{R}_{>0}$ such that $\mathcal{M}(\mathbf{x} + \delta_1\mathbb{B}) \subset \epsilon_1\mathbb{B}$ by local boundedness of $\mathcal{M}_1$ relative to $\mathcal{A}_1$ and by openness of $\mathcal{A}_1 \setminus \mathcal{A}_2$ relative to $\mathcal{A}_1$. Similar argument holds for each $\mathbf{x} \in \mathcal{A}_2 \setminus \mathcal{A}_1$. For each $\mathbf{x} \in \mathcal{A}_1 \cap \mathcal{A}_2$, choose $\delta := \min\{\delta_1, \delta_2\} \in \mathbb{R}_{>0}$ and $\epsilon := \max\{\epsilon_1, \epsilon_2\} \in \mathbb{R}_{>0}$ such that $\delta_1, \delta_2, \epsilon_1, \epsilon_2$ comes from the local boundedness property of $\mathcal{M}_1$ and $\mathcal{M}_2$, we have that $\mathcal{M}(\mathbf{x} + \delta\mathbb{B}) \subset \epsilon\mathbb{B}$, which concludes the proof. ∎

Remark 5. The requirement of closedness of $\mathcal{A}_1, \mathcal{A}_2$ relative to $\mathbb{R}^n$ is essential. Consider the following example. $\mathcal{M}_1 : \mathbb{R} \rightrightarrows \mathbb{R}$ such that $\mathcal{M}_1(x) := \left\{\frac{1}{x}\right\}$ for each $x \in \mathcal{A}_1 :=]0, 1]$, $\mathcal{M}_2 : \mathbb{R} \rightrightarrows \mathbb{R}$ such that $\mathcal{M}_2(x) := \{0\}$ for each $x \in \mathcal{A}_2 := [0, 1[$, $\mathcal{M}$

is neither outer semicontinuous nor locally bounded relative to $\mathcal{A}_1 \cup \mathcal{A}_2 = [0,1]$, despite the fact that for each $i \in \{1,2\}$ we have that $\mathcal{M}_i$ is both outer semicontinuous and locally bounded relative to $\mathcal{A}_i$.

APPENDIX B

Proof of Lemma 2. The following proof is inspired by lemma 2.7 in the work of Sanfelice et al.[34] Local boundedness of $\mathcal{F}$ relative to C implies that for each compact set $\mathcal{A} \subset C$, there exists a compact set $\mathcal{A}' \subset \mathbb{R}^n$, such that $\mathcal{F}(\mathcal{A}) \subset \mathcal{A}'$. By precompactness of $\boldsymbol{\phi}$, there exists some $a \in \mathbb{R}_{>0}$, such that $\mathcal{F}\left(\operatorname{rge} \boldsymbol{\phi}\right) \subset a\mathbb{B}$, which implies that $\left|\dot{\boldsymbol{\phi}}(t,j)\right| < a$ for each $(t,j) \in \operatorname{dom} \boldsymbol{\phi}$. Let $\mathcal{E} := \left\{ \bigcup_{j=0}^{J-1} \left(t_{j+1}, j\right) : \left(t_{j+1}, j\right) \in \operatorname{dom} \boldsymbol{\phi} \right\}$, where $J = \sup\{j \in \mathbb{Z}_{\geq 0} : \exists\, t \in \mathbb{R}_{\geq 0}, (t,j) \in \operatorname{dom} \boldsymbol{\phi}\}$, be the set of all points when a jump occurs such that $\mathcal{E} \neq \emptyset$ (otherwise $\boldsymbol{\phi}$ would undergo no jumps at all so that it is not Zeno). Then $\boldsymbol{\phi}(\mathcal{E}) \subset \mathcal{D}$, $\overline{\boldsymbol{\phi}(\mathcal{E})}$ is nonempty and compact by precompactness of $\boldsymbol{\phi}$, and $\overline{\boldsymbol{\phi}(\mathcal{E})} \subset \mathcal{D}$ due to the fact that $\mathcal{D}$ is closed relative to $\mathbb{R}^n$. Outer semicontinuity of $\mathcal{G}$ relative to $\mathcal{D}$ implies that the set $\mathcal{G}\left(\overline{\boldsymbol{\phi}(\mathcal{E})}\right)$ is compact. By similar arguments as above, $\mathcal{G}^k\left(\overline{\boldsymbol{\phi}(\mathcal{E})}\right) \subset \mathcal{G}(\mathcal{D})$ is compact for each $k \in \mathbb{Z}_{>0}$. By (3), $\mathcal{G}^K\left(\overline{\boldsymbol{\phi}(\mathcal{E})}\right) \cap \overline{\boldsymbol{\phi}(\mathcal{E})} = \emptyset$. Then, the distance between the two sets $\mathcal{G}^K\left(\overline{\boldsymbol{\phi}(\mathcal{E})}\right)$ and $\overline{\boldsymbol{\phi}(\mathcal{E})}$ is positive or positively infinite, that is, there exists some $b \in \mathbb{R}_{>0} \cup \{\infty\}$ such that $b = \inf\left\{ |\mathbf{w} - \mathbf{v}| : \mathbf{w} \in \mathcal{G}^K\left(\overline{\boldsymbol{\phi}(\mathcal{E})}\right), \mathbf{v} \in \overline{\boldsymbol{\phi}(\mathcal{E})} \right\}$. It follows that the distance between t_j and t_{j+K+1} is at least $\frac{b}{a} \in \mathbb{R}_{>0} \cup \{\infty\}$ for each $j \in \{0, 1, \ldots, J-1\}$. If J is finite, then $\boldsymbol{\phi}$ is not Zeno. If J is infinite, then for each $c \in \mathbb{R}_{>0}$, there exists a finite $J' = \lceil \frac{ac}{b}(K+1) \rceil + 1$ such that $t_{J'} > \frac{b}{a} \lfloor \frac{J'}{K+1} \rfloor > c$, where the functions $\lceil x \rceil := \min\{y \in \mathbb{Z} : y \geq x\}$ and $\lfloor x \rfloor := \max\{y \in \mathbb{Z} : y \leq x\}$ for each $x \in \mathbb{R}$. Therefore, $\sup_t(\operatorname{dom} \boldsymbol{\phi}) = \infty$, which implies that $\boldsymbol{\phi}$ is not Zeno. ∎

APPENDIX C

Proof of Lemma 4. The unique equilibrium point for the system (13) is the origin. Positive definiteness of $\overline{V}$ is due to the fact that $\overline{V}(\mathbf{z}) > 0$ for each $\mathbf{z} \in \mathbb{R}^6 \setminus \{\mathbf{0}\}$ and $\overline{V}(\mathbf{0}) = 0$. To check radial unboundedness of $\overline{V}$, observe that $\overline{V}(\mathbf{z}) = \sum_{i=1}^3 \frac{k_{\mathbf{v}}\gamma}{2k_{\mathbf{p}}}(\beta_i(\kappa_i(\mathbf{z})) - \frac{k_{\mathbf{p}}}{k_{\mathbf{v}}}\mathbf{e}_i^\top \mathbf{z}_2)^2 + (k_{\mathbf{v}} - \gamma)\frac{k_{\mathbf{p}}}{2k_{\mathbf{v}}}|\mathbf{z}_2|^2 + \sum_{i=1}^3 \int_0^{\kappa_i(\mathbf{z})} \beta_i(\tau)d\tau \geq (k_{\mathbf{v}} - \gamma)\frac{k_{\mathbf{p}}}{2k_{\mathbf{v}}}|\mathbf{z}_2|^2 + \sum_{i=1}^3 \int_0^{\kappa_i(\mathbf{z})} \beta_i(\tau)d\tau$. We proceed by contradiction. Suppose $\overline{V}$ is not radially unbounded, then $\overline{V}$ is bounded on $\mathbb{R}^6$. This implies that $|\mathbf{z}_2|$ remains bounded as $|\mathbf{z}| \to \infty$, therefore $|\mathbf{z}_1| \to \infty$ as $|\mathbf{z}| \to \infty$. Now, $\kappa_i(\mathbf{z}) \to \pm\infty$ as $|\mathbf{z}| \to \infty$ for some $i \in \{1,2,3\}$. For this particular i, there exists $\xi \in \mathbb{R} \setminus \{0\}$ such that $\lim_{|\mathbf{z}|\to\infty} \overline{V}(\mathbf{z}) \geq \lim_{|\mathbf{z}|\to\infty} \int_0^{\kappa_i(\mathbf{z})} \beta_i(\tau)d\tau > \lim_{|\mathbf{z}|\to\infty} \int_\xi^{\kappa_i(\mathbf{z})} \beta_i(\tau)d\tau > \lim_{|\mathbf{z}|\to\infty} \int_\xi^{\kappa_i(\mathbf{z})} \beta_i(\xi)d\tau = \lim_{|\mathbf{z}|\to\infty} |\beta_i(\xi)(\kappa_i(\mathbf{z}) - \xi)| = \infty$. This contradicts with the premise that $\overline{V}$ is not radially unbounded. Moreover, we have that

$$\left\langle \nabla \overline{V}(\mathbf{z}), \begin{bmatrix} \mathbf{z}_2 \\ -\boldsymbol{\beta}(\boldsymbol{\kappa}(\mathbf{z})) \end{bmatrix} \right\rangle = -\sum_{i=1}^3 ((k_{\mathbf{v}} - \gamma)\beta_i(\kappa_i(\mathbf{z}))^2 + \frac{\gamma}{k_{\mathbf{p}}} \nabla \beta_i(\kappa_i(\mathbf{z}))(k_{\mathbf{p}}\mathbf{e}_i^\top \mathbf{z}_2 - k_{\mathbf{v}}\beta_i(\kappa_i(\mathbf{z}))^2) \leq 0,$$

for each $\mathbf{z} \in \mathbb{R}^6$, wherein the equality holds if and only if $\mathbf{z} = \mathbf{0}$ due to the choice of γ and by the property (9a). ∎

APPENDIX D

With the definition of $\mathbf{r}_{3d}$ given in (11) satisfying the inequality (10), it is eligible to define $\mathbf{r}_{3d} = \boldsymbol{\nu} \circ \boldsymbol{\mu}$, where $\boldsymbol{\nu}(\mathbf{s}) := \frac{\mathbf{s}}{|\mathbf{s}|}$ for each $\mathbf{s} \in \mathbb{R}^3 \setminus \{\mathbf{0}\}$, such that

$$\begin{aligned} \dot{\mathbf{r}}_{3d} &= J_{\mathbf{r}_{3d}}(\mathbf{r}, \mathbf{z}) \begin{bmatrix} \dot{\mathbf{r}} \\ \dot{\mathbf{z}} \end{bmatrix} \\ &= J_{\boldsymbol{\nu}}(\boldsymbol{\mu}(\mathbf{r}, \mathbf{z}))\, J_{\boldsymbol{\mu}}(\mathbf{r}, \mathbf{z}) \begin{bmatrix} \dot{\mathbf{r}} \\ \dot{\mathbf{z}} \end{bmatrix}, \end{aligned} \tag{D1}$$

where $J_\nu(\boldsymbol{\mu}(\mathbf{r},\mathbf{z})) = J_\nu(\mathbf{s})|_{\mathbf{s}=\boldsymbol{\mu}(\mathbf{r},\mathbf{z})} = -\frac{S(\mathbf{s})^2}{|\mathbf{s}|^3}\Big|_{\mathbf{s}=\boldsymbol{\mu}(\mathbf{r},\mathbf{z})}$, $J_{\boldsymbol{\mu}}(\mathbf{r},\mathbf{z}) = \begin{bmatrix}0_{3\times 6} & -I_3 & J_\beta(\boldsymbol{\kappa}(\mathbf{z}))J_{\boldsymbol{\kappa}}(\mathbf{z})\end{bmatrix}$, $J_{\boldsymbol{\kappa}}(\mathbf{z}) = \begin{bmatrix}k_{\mathbf{p}}I_3 & k_{\mathbf{v}}I_3\end{bmatrix}$, $\dot{\mathbf{r}} = \mathbf{f}_d(\mathbf{r},\mathbf{p}_d^{(3)})$ for some $\mathbf{p}_d^{(3)} \in r\overline{\mathbb{B}}$, and $\dot{\mathbf{z}} = \begin{bmatrix}\mathbf{z}_2 \\ -\frac{1}{m}\mathbf{r}_3 T(\mathbf{r},\mathbf{z},\mathbf{r}_3) + g\mathbf{e}_3 - \ddot{\mathbf{p}}_d\end{bmatrix}$. Then, (D1) can be rewritten as

$$\dot{\mathbf{r}}_{3d} = -\frac{S(\mathbf{r}_{3d}(\mathbf{r},\mathbf{z}))^2}{|\boldsymbol{\mu}(\mathbf{r},\mathbf{z})|}(J_\beta(\boldsymbol{\kappa}(\mathbf{z}))(k_{\mathbf{p}}\mathbf{z}_2 - k_{\mathbf{v}}(\boldsymbol{\beta}(\boldsymbol{\kappa}(\mathbf{z})) + S(\mathbf{r}_3)^2\boldsymbol{\mu}(\mathbf{r},\mathbf{z}))) - \mathbf{p}_d^{(3)}).$$

Therefore, the desired angular velocity can be chosen to be (18) such that $\breve{\boldsymbol{\omega}}_d$ satisfies the equation $\dot{\mathbf{r}}_{3d} = -S(\mathbf{r}_{3d}(\mathbf{r},\mathbf{z}))\breve{\boldsymbol{\omega}}_d(\mathbf{r},\mathbf{z},\mathbf{r}_3,\mathbf{p}_d^{(3)})$.

APPENDIX E

Proof of Lemma 5. Firstly, we prove that $\mathcal{H}_0$ meets the hybrid basic conditions.[30] Continuity of the function $(\mathbf{r},\mathbf{z},\mathbf{r}_3) \mapsto \min_{\rho\in\mathcal{Q}} V_\rho(\mathbf{r},\mathbf{z},\mathbf{r}_3)$ follows from theorem 9.14 in the work of Sundaram et al.[40] by continuity of the function (16) and compactness of the set $\mathcal{Q}$. Being the pre-image of closed subsets by the continuous function $\mathbf{x}_0 \mapsto \Delta(\mathbf{x}_0)$, both $\mathcal{C}_0$ and $\mathcal{D}_0$ are closed relative to $\mathbb{R}^{19}$, thanks to relative closedness of $\mathcal{S}_{\mathbf{x}_0}$ to $\mathbb{R}^{19}$. By continuity of $\mathbf{f}_d$, $\mathbf{f}$, T, and $\breve{\boldsymbol{\omega}}$ and by compactness of $r\overline{\mathbb{B}}$, $\mathcal{F}_0$ is convex-valued, outer semicontinuous and locally bounded relative to $\mathcal{C}_0$. Similarly, $\mathcal{G}_0$ is outer semicontinuous and locally bounded relative to $\mathcal{D}_0$.

Secondly, we prove that each maximal solution to $\mathcal{H}_0$ is precompact by proposition 6.10 in the work of Goebel et al.[30] Since $\mathcal{C}_0 \cup \mathcal{D}_0 = \mathcal{S}_{\mathbf{x}_0}$ and that $\mathcal{C}_0 \setminus \mathcal{D}_0$ is open relative to $\mathcal{S}_{\mathbf{x}_0}$, we have that $\mathcal{T}_{\mathcal{C}_0}(\mathbf{x}_0) = \mathcal{T}_{\mathcal{S}_{\mathbf{x}_0}}(\mathbf{x}_0) = \mathcal{T}_{\mathcal{S}_d}(\mathbf{r}) \times \mathbb{R}^6 \times \{\mathbf{w}\in\mathbb{R}^3 : \langle \mathbf{w},\mathbf{r}_3\rangle = 0\} \times \{0\}$ for each $\mathbf{x}_0 \in \mathcal{C}_0 \setminus \mathcal{D}_0$. Together with (6), it implies that the viability condition (VC), $\mathcal{F}_0(\mathbf{x}_0) \cap \mathcal{T}_{\mathcal{C}_0}(\mathbf{x}_0) \neq \emptyset$, holds for each $\mathbf{x}_0 \in \mathcal{C}_0 \setminus \mathcal{D}_0$. For each $\mathbf{x}_0(0,0) \in \mathcal{S}_{\mathbf{x}_0}$, the set

$$\mathcal{U}_0 := \{\mathbf{x}_0 \in \mathcal{S}_{\mathbf{x}_0} : V_q(\mathbf{r},\mathbf{z},\mathbf{r}_3) \leq V_{q(0,0)}(\mathbf{r}(0,0),\mathbf{z}(0,0),\mathbf{r}_3(0,0))\}, \tag{E1}$$

is compact due to compactness of the sets $\mathcal{S}_d$, $\mathbb{S}^2$, and $\mathcal{Q}$, and due to the fact that the function $\mathbf{x}_0 \mapsto V_q(\mathbf{r},\mathbf{z},\mathbf{r}_3)$ is positive definite to the compact set $\mathcal{A}_0$ while tending to infinity as $|\mathbf{z}|\to\infty$. For each $\mathbf{x}_0 \in \mathcal{C}_0$ and for each $\mathbf{u}_0 \in \mathcal{F}_0(\mathbf{x}_0)$, $\left\langle \nabla V_q(\mathbf{r},\mathbf{z},\mathbf{r}_3), \mathbf{u}_0 \right\rangle = W(\mathbf{r},\mathbf{z},\mathbf{r}_3)$, given in (20). Defining

$$u_{\mathcal{C}_0}(\mathbf{x}_0) := \begin{cases} W(\mathbf{r},\mathbf{z},\mathbf{r}_3) & \text{if} \quad \mathbf{x}_0 \in \mathcal{C}_0, \\ -\infty & \text{otherwise,} \end{cases}$$

we have that $\left\langle \nabla V_q(\mathbf{r},\mathbf{z},\mathbf{r}_3), \mathbf{u}_0 \right\rangle \leq u_{\mathcal{C}_0}(\mathbf{x}_0) \leq 0$ for each $\mathbf{x}_0 \in \mathcal{U}_0 \cap \mathcal{C}_0$ and for each $\mathbf{u}_0 \in \mathcal{F}_0(\mathbf{x}_0)$. On one hand, $u_{\mathcal{C}_0}(\mathbf{x}_0) = 0$ for each $\mathbf{x}_0 \in \mathcal{A}_0$. On the other hand, $W(\mathbf{r},\mathbf{z},\mathbf{r}_3) = 0$ if and only if $\mathbf{x}_0 \in \left\{\mathbf{x}_0 \in \mathcal{S}_{\mathbf{x}_0} : \mathbf{z} = \mathbf{0}, \mathbf{r}_3 = \pm\left(g\mathbf{e}_3 - \ddot{\mathbf{p}}_d\right)/|g\mathbf{e}_3 - \ddot{\mathbf{p}}_d|\right\}$, but the choice $\mathbf{x}_0 = (\mathbf{r},\mathbf{0},-q\left(g\mathbf{e}_3 - \ddot{\mathbf{p}}_d\right)/|g\mathbf{e}_3 - \ddot{\mathbf{p}}_d|, q)$ leads to $\Delta(\mathbf{x}_0) = 2\epsilon$ so that $\mathbf{x}_0 \notin \mathcal{C}_0$. Thus $u_{\mathcal{C}_0}^{-1}(0) = \mathcal{A}_0$. For each $\mathbf{x}_0 \in \mathcal{D}_0$, let $\mathbf{x}_0^+ = \mathcal{G}_0(\mathbf{x}_0)$, then $V_{q^+}(\mathbf{r}^+,\mathbf{z}^+,\mathbf{r}_3^+) - V_q(\mathbf{r},\mathbf{z},\mathbf{r}_3) = 2\epsilon q\mathbf{r}_3^\top\mathbf{r}_{3d}(\mathbf{r},\mathbf{z})$. Defining

$$u_{\mathcal{D}_0}(\mathbf{x}_0) := \begin{cases} 2\epsilon q\mathbf{r}_3^\top\mathbf{r}_{3d}(\mathbf{r},\mathbf{z}) & \text{if} \quad \mathbf{x}_0 \in \mathcal{D}_0, \\ -\infty & \text{otherwise,} \end{cases}$$

we have that $V_{q^+}(\mathbf{r}^+,\mathbf{z}^+,\mathbf{r}_3^+) - V_q(\mathbf{r},\mathbf{z},\mathbf{r}_3) \leq u_{\mathcal{D}_0}(\mathbf{x}_0) < 0$ for each $\mathbf{x}_0 \in \mathcal{U}_0 \cap \mathcal{D}_0$. Note that $u_{\mathcal{D}_0}(\mathbf{x}_0) = 0$ if and only if $\mathbf{x}_0 \in \{\mathbf{x}_0 \in \mathcal{D}_0 : \langle \mathbf{r}_3, q\mathbf{r}_{3d}\rangle = 0\}$, but now $\Delta(\mathbf{x}_0) = 0$ so that $\mathbf{x}_0 \notin \mathcal{D}_0$. Thus $u_{\mathcal{D}_0}^{-1}(0) = \emptyset$. Since the function $\mathbf{x}_0 \mapsto V_q(\mathbf{r},\mathbf{z},\mathbf{r}_3)$ is nonincreasing along each maximal solution $\mathbf{x}_0$ to $\mathcal{H}_0$, we have that $\mathbf{x}_0(t,j) \in \mathcal{U}_0$ for each $(t,j) \in \operatorname{dom}\mathbf{x}_0$, which implies boundedness of $\mathbf{x}_0$. In addition, the fact that $\mathcal{G}_0(\mathcal{D}_0) \subset \mathcal{C}_0 \setminus \mathcal{D}_0 \subset \mathcal{S}_{\mathbf{x}_0} = \mathcal{C}_0 \cup \mathcal{D}_0$ lets us conclude precompactness of each maximal solution to $\mathcal{H}_0$.

We are now in the conditions of case (i) of corollary 8.9 in the work of Goebel et al.,[30] where $u_{\mathcal{C}_0}(\mathbf{x}_0) < 0$ and $u_{\mathcal{D}_0}(\mathbf{x}_0) < 0$ for each $\mathbf{x}_0 \in \mathcal{U}_0 \setminus \mathcal{A}_0$, and the desired conclusion follows. ∎

APPENDIX F

Proof of Theorem 1. In proving closedness of the flow set and the jump set, notice that $\mathcal{F}$ is convex-valued, compact-valued, outer semicontinuous and locally bounded relative to $\mathcal{C}$. It follows from lemma 5.15 in the work of Goebel et al.[30] that

$\mathcal{F}$ is upper semicontinuous at each $\mathbf{x} \in \mathcal{C}$ and from proposition 9.9 in the work of Sundaram et al.[40] that $\mathcal{F}$ is lower semicontinuous at each $\mathbf{x} \in \mathcal{C}$. By theorem 9.14 in the work of Sundaram et al.,[40] the function $\mathbf{x} \mapsto \max_{\mathbf{u}\in\mathcal{F}(\mathbf{x})} \left\langle \nabla \widetilde{V}_q(\mathbf{x}), \mathbf{u} \right\rangle$ is continuous on $\mathcal{S}_{\mathbf{x}}$, which implies that both $\mathcal{C}$ and $\mathcal{D}$ are closed relative to $\mathbb{R}^{23}$. By the construction of $\mathcal{G}_1$ in (24) and $\mathcal{G}_2$ in (25), we have that $\mathcal{G}$ is in the form of (2) in Lemma 1. Outer semicontinuity and local boundedness of $\mathcal{G}$ relative to $\mathcal{D}$ then follows.

In proving precompactness of each maximal solution to $\mathcal{H}$ by proposition 6.10 in the work of Goebel et al.,[30] observe that $\mathcal{C} \cup \mathcal{D} = \mathcal{S}_{\mathbf{x}}$ and that $\mathcal{C} \setminus \mathcal{D}$ is open relative to $\mathcal{S}_{\mathbf{x}}$, then $\mathcal{T}_{\mathcal{C}}(\mathbf{x}) = \mathcal{T}_{\mathcal{S}_{\mathbf{x}}}(\mathbf{x}) = \mathcal{T}_{\mathcal{S}_d}(\mathbf{r}) \times \mathbb{R}^6 \times \{\mathbf{w} \in \mathbb{R}^3 : \langle \mathbf{w}, \mathbf{r}_3 \rangle = 0\} \times \{0\} \times \mathbb{R}^4$ for each $\mathbf{x} \in \mathcal{C} \setminus \mathcal{D}$. Together with (6), it implies that the viability condition (VC), $\mathcal{F}(\mathbf{x}) \cap \mathcal{T}_{\mathcal{C}}(\mathbf{x}) \neq \emptyset$, holds for each $\mathbf{x} \in \mathcal{C} \setminus \mathcal{D}$. Let $\mathcal{U} := \mathcal{U}_0 \times \mathbb{R} \times \mathbb{R}^3$ with $\mathcal{U}_0$ defined in (E1). Defining

$$u_{\mathcal{C}}(\mathbf{x}) := \begin{cases} \max\limits_{\mathbf{u}\in\mathcal{F}(\mathbf{x})} \left\langle \nabla \widetilde{V}_q(\mathbf{x}), \mathbf{u} \right\rangle & \text{if} \quad \mathbf{x} \in \mathcal{C}, \\ -\infty & \text{otherwise}, \end{cases}$$

we have that $\left\langle \nabla \widetilde{V}_q(\mathbf{x}), \mathbf{u} \right\rangle \leq u_{\mathcal{C}}(\mathbf{x}) \leq \sigma\widetilde{W}(\mathbf{x}) \leq 0$ for each $\mathbf{x} \in \mathcal{U} \cap \mathcal{C}$ and for each $\mathbf{u} \in \mathcal{F}(\mathbf{x})$. On one hand, $u_{\mathcal{C}}(\mathbf{x}) = 0$ for each $\mathbf{x} \in \mathcal{A}$. On the other hand, $\max_{\mathbf{u}\in\mathcal{F}(\mathbf{x})} \left\langle \nabla \widetilde{V}_q(\mathbf{x}), \mathbf{u} \right\rangle = 0$ implies $\widetilde{W}(\mathbf{x}) = 0$, which is true if and only if $\mathbf{x} \in \left\{\mathbf{x} \in \mathcal{S}_{\mathbf{x}} : \mathbf{z} = \mathbf{0}, \mathbf{r}_3 = \pm \left(g\mathbf{e}_3 - \ddot{\mathbf{p}}_d\right)/|g\mathbf{e}_3 - \ddot{\mathbf{p}}_d|\right\}$, but the choice $\mathbf{x} = (\mathbf{r}, \mathbf{0}, -q\left(g\mathbf{e}_3 - \ddot{\mathbf{p}}_d\right)/|g\mathbf{e}_3 - \ddot{\mathbf{p}}_d|, q, s_1, \mathbf{s}_2)$ leads to $\Delta(\mathbf{x}_0) = 2\epsilon$ so that $\mathbf{x} \notin \mathcal{C}$. Thus $u_{\mathcal{C}}^{-1}(0) = \mathcal{A}$. Defining

$$u_{\mathcal{D}}(\mathbf{x}) := \begin{cases} 2\epsilon q \mathbf{r}_3^{\top} \mathbf{r}_{3d}(\mathbf{r}, \mathbf{z}) & \text{if} \quad \mathbf{x} \in \mathcal{D}_1 \setminus \mathcal{D}_2, \\ 0 & \text{if} \quad \mathbf{x} \in \mathcal{D}_2, \\ -\infty & \text{otherwise}, \end{cases}$$

we have that $\widetilde{V}_{q^+}(\mathbf{x}^+) - \widetilde{V}_q(\mathbf{x}) \leq u_{\mathcal{D}}(\mathbf{x}) \leq 0$ for each $\mathbf{x} \in \mathcal{U} \cap \mathcal{D}$. Note that $u_{\mathcal{D}}(\mathbf{x}) = 0$ if and only if $\mathbf{x} \in \{\mathbf{x} \in \mathcal{D}_1 \setminus \mathcal{D}_2 : \langle \mathbf{r}_3, q\mathbf{r}_{3d} \rangle = 0\} \cup \mathcal{D}_2$, but now $\Delta(\mathbf{x}_0) = 0$ so that $\mathbf{x} \notin \mathcal{D}_1$. Thus $u_{\mathcal{D}}^{-1}(0) = \mathcal{D}_2$. Since the function $\mathbf{x} \mapsto \widetilde{V}_q(\mathbf{x})$ is nonincreasing along each maximal solution $\mathbf{x}$ to $\mathcal{H}$, $\mathbf{x}(t,j) \in \mathcal{U}$ for each $(t,j) \in \operatorname{dom} \mathbf{x}$. Let $\mathcal{E} := \left\{\bigcup_{j=0}^{J-1} \left(t_{j+1}, j\right) : \left(t_{j+1}, j\right) \in \operatorname{dom} \mathbf{x}\right\}$, where $J = \sup\{j \in \mathbb{Z}_{\geq 0} : \exists\, t \in \mathbb{R}_{\geq 0}, (t,j) \in \operatorname{dom} \mathbf{x}\}$, be the set of all points when a jump occurs. Following (23), the value of $(s_1, \mathbf{s}_2)$ remains constant on jumping through $\mathcal{G}_1$ or during flow, and is updated to the value of $(T, \breve{\boldsymbol{\omega}})$ on jumping through $\mathcal{G}_2$. Hence, $\operatorname{rge}(s_1, \mathbf{s}_2) \subset \mathcal{S} := \{(s_1(0,0), \mathbf{s}_2(0,0))\} \cup (\{T(\mathbf{r}(t,j), \mathbf{z}(t,j), \mathbf{r}_3(t,j)) : (t,j) \in \mathcal{E}\} \times \{\breve{\boldsymbol{\omega}}\left(\mathbf{x}_0(t,j), \mathbf{p}_d^{(3)}(t,j)\right) : (t,j) \in \mathcal{E}\})$. Since $\mathcal{E} \subset \operatorname{dom} \mathbf{x}$, we further have that $\mathcal{S} \subset \{(s_1(0,0), \mathbf{s}_2(0,0))\} \cup (T(\operatorname{rge}(\mathbf{r}, \mathbf{z}, \mathbf{r}_3)) \times \breve{\boldsymbol{\omega}}(\mathcal{U}_0 \times r\overline{\mathbb{B}}))$. By continuity of $(T, \breve{\boldsymbol{\omega}})$ and compactness of $\mathcal{U}_0$, we conclude boundedness of $(s_1, \mathbf{s}_2)$ and therefore boundedness of $\mathbf{x}$. It can be further verified that

$$\begin{cases} \mathcal{G}(\mathcal{D}_1 \setminus \mathcal{D}_2) & \subset \mathcal{C}_1 \setminus \mathcal{D}_1, \\ \mathcal{G}(\mathcal{D}_2 \setminus \mathcal{D}_1) & \subset \mathcal{C} \setminus \mathcal{D}_1, \\ \mathcal{G}(\mathcal{D}_1 \cap \mathcal{D}_2) & \subset \mathcal{S}_{\mathbf{x}} \setminus (\mathcal{D}_1 \cap \mathcal{D}_2). \end{cases}$$

As a result, $\mathcal{G}(\mathcal{D}) \subset \mathcal{S}_{\mathbf{x}} = \mathcal{C} \cup \mathcal{D}$ and we conclude precompactness of each maximal solution to $\mathcal{H}$.

In proving global attractivity of $\mathcal{A}$ for $\mathcal{H}$, recall from previous paragraph that $u_{\mathcal{C}}^{-1}(0) = \mathcal{A}$, $u_{\mathcal{D}}^{-1}(0) = \mathcal{D}_2$, so that we obtain $\mathcal{G}(u_{\mathcal{D}}^{-1}(0)) \subset \mathcal{S}_{\mathbf{x}} \setminus (\mathcal{D}_1 \cap \mathcal{D}_2)$. It follows from corollary 8.4 in the work of Goebel et al.[30] that for some $\xi \in \mathbb{R}_{\geq 0}$, each precompact solution to $\mathcal{H}$ approaches the nonempty set $\mathcal{W}$ which is the largest weakly invariant subset of $\widetilde{V}_q^{-1}(\xi) \cap (\mathcal{A} \cup (\mathcal{D}_2 \setminus \mathcal{D}_1))$. Since $\mathcal{G}(\mathbf{x}) \subset \mathcal{C} \setminus \mathcal{D}$ for each $\mathbf{x} \in (\mathcal{D}_2 \setminus \mathcal{D}_1) \setminus \mathcal{A}$, then $(\mathcal{D}_2 \setminus \mathcal{D}_1) \setminus \mathcal{A}$ cannot be weakly invariant and thus $\mathcal{W} \subset \widetilde{V}_q^{-1}(\xi) \cap (\mathcal{A} \setminus (\mathcal{D}_2 \setminus \mathcal{D}_1))$. Hence, $\mathcal{W} \subset \mathcal{A}$ and global attractivity of $\mathcal{A}$ for $\mathcal{H}$ follows.

In proving stability of $\mathcal{A}$ for $\mathcal{H}$, notice that there exist α_1, α_2 of class $\mathcal{K}_\infty$ such that $\alpha_1\left(|\mathbf{x}_0|_{\mathcal{A}_0}\right) \leq V_q(\mathbf{r}, \mathbf{z}, \mathbf{r}_3) \leq \alpha_2\left(|\mathbf{x}_0|_{\mathcal{A}_0}\right)$ for each $\mathbf{x}_0 \in \mathcal{S}_{\mathbf{x}_0}$ by lemma 3 from Postoyan et al.[16] Now $|\mathbf{x}|_{\mathcal{A}} = |\mathbf{x}_0|_{\mathcal{A}_0}$ for each $\mathbf{x} \in \mathcal{S}_{\mathbf{x}}$, so that the functions of $\mathcal{K}_\infty$ used to lower and upper bound the Lyapunov function candidate $\mathbf{x} \mapsto \widetilde{V}_q(\mathbf{x})$ can be chosen to be the same as α_1 and α_2. The fact that $\mathbf{x} \mapsto \widetilde{V}_q(\mathbf{x})$ is nonincreasing along each maximal solution $\mathbf{x}$ to $\mathcal{H}$ yields $\alpha_1(|\mathbf{x}(t,j)|_{\mathcal{A}}) \leq \widetilde{V}_{q(t,j)}(\mathbf{x}(t,j)) \leq \widetilde{V}_{q(0,0)}(\mathbf{x}(0,0)) \leq \alpha_2(|\mathbf{x}(0,0)|_{\mathcal{A}})$, and consequently, $|\mathbf{x}(t,j)|_{\mathcal{A}} \leq \alpha_1^{-1}(\alpha_2(|\mathbf{x}(0,0)|_{\mathcal{A}}))$ for each $(t,j) \in \operatorname{dom} \mathbf{x}$. Therefore, $\mathcal{A}$ is stable for $\mathcal{H}$. ∎

APPENDIX G

Proof of Corollary. 1 This proof follows similar lines as the proof of Theorem 1 with major differences highlighted below.

In proving that $\widehat{\mathcal{H}}$ meets the hybrid basic conditions, notice that both $\widehat{\mathcal{C}} := \widehat{\mathcal{C}}_1 \cap \widehat{\mathcal{C}}_2$ and $\widehat{\mathcal{D}} := \widehat{\mathcal{D}}_1 \cup \widehat{\mathcal{D}}_2$ are closed relative to $\mathbb{R}^{23}$ by closedness of $\widehat{\mathcal{A}}$ relative to $\mathbb{R}^{23}$, while both outer semicontinuity and local boundedness of $\widehat{\mathcal{F}}, \widehat{\mathcal{G}}$ relative to $\widehat{\mathcal{C}}, \widehat{\mathcal{D}}$ maintain, respectively.

In proving precompactness of each maximal solution to $\widehat{\mathcal{H}}$, consider the Lyapunov function candidate $\widehat{V}_q : \mathbb{R}^{23} \to \mathbb{R}$ defined as $\mathbf{x} \mapsto \max\{0, \widetilde{V}_q(\mathbf{x}) - \delta\}$, which is locally Lipschitz on some open set containing $\mathcal{S}_{\mathbf{x}}$. Defining

$$u_{\widehat{\mathcal{C}}}(\mathbf{x}) := \begin{cases} \max\limits_{\mathbf{u} \in \mathcal{F}(\mathbf{x})} \widehat{V}_q^\circ(\mathbf{x}; \mathbf{u}) & \text{if} \quad \mathbf{x} \in \widehat{\mathcal{C}}, \\ -\infty & \text{otherwise}, \end{cases}$$

where $\widehat{V}_q^\circ(\mathbf{x}; \mathbf{u})$ denotes the generalized directional derivative of Clarke of $\widehat{V}_q$ at $\mathbf{x}$ in the direction $\mathbf{u}$, that is, $\widehat{V}_q^\circ(\mathbf{x}; \mathbf{u}) := \limsup_{h \to 0^+,\ \mathbf{y} \to \mathbf{x}} (\widehat{V}_q(\mathbf{y} + h\mathbf{u}) - \widehat{V}_q(\mathbf{y}))/h$, we resort to lemma 1 from Postoyan et al.[16] to conclude that $\widehat{V}_q^\circ(\mathbf{x}; \mathbf{u}) \leq u_{\widehat{\mathcal{C}}}(\mathbf{x}) \leq 0$ for each $\mathbf{x} \in \mathcal{U} \cap \widehat{\mathcal{C}}$ and for each $\mathbf{u} \in \mathcal{F}(\mathbf{x})$. On one hand, $u_{\widehat{\mathcal{C}}}(\mathbf{x}) = 0$ for each $\mathbf{x} \in \widehat{\mathcal{A}}$. On the other hand, $\max_{\mathbf{u} \in \mathcal{F}(\mathbf{x})} \langle \nabla \widetilde{V}_q(\mathbf{x}), \mathbf{u} \rangle = 0$ implies $\widetilde{W}(\mathbf{x}) = 0$, which is true if and only if $\mathbf{x} \in \{\mathbf{x} \in \mathcal{S}_{\mathbf{x}} : \mathbf{z} = \mathbf{0}, \mathbf{r}_3 = \pm(g\mathbf{e}_3 - \ddot{\mathbf{p}}_d)/|g\mathbf{e}_3 - \ddot{\mathbf{p}}_d|\}$, but the choice $\mathbf{x} = (\mathbf{r}, \mathbf{0}, -q(g\mathbf{e}_3 - \ddot{\mathbf{p}}_d)/|g\mathbf{e}_3 - \ddot{\mathbf{p}}_d|, q, s_1, \mathbf{s}_2)$ leads to $\Delta(\mathbf{x}_0) = 2\epsilon$ so that $\mathbf{x} \notin \mathcal{C}$. Thus $u_{\widehat{\mathcal{C}}}^{-1}(0) = \widehat{\mathcal{A}}$. Defining

$$u_{\widehat{\mathcal{D}}}(\mathbf{x}) := \begin{cases} 2\epsilon q \mathbf{r}_3^\top \mathbf{r}_{3d}(\mathbf{r}, \mathbf{z}) & \text{if} \quad \mathbf{x} \in \widehat{\mathcal{D}}_1 \setminus \widehat{\mathcal{D}}_2, \\ 0 & \text{if} \quad \mathbf{x} \in \widehat{\mathcal{D}}_2, \\ -\infty & \text{otherwise}, \end{cases}$$

we have that $\widehat{V}_{q^+}(\mathbf{x}^+) - \widehat{V}_q(\mathbf{x}) \leq u_{\widehat{\mathcal{D}}}(\mathbf{x}) \leq 0$ for each $\mathbf{x} \in \mathcal{U} \cap \widehat{\mathcal{D}}$. Note that $u_{\widehat{\mathcal{D}}}(\mathbf{x}) = 0$ if and only if $\mathbf{x} \in \{\mathbf{x} \in \widehat{\mathcal{D}}_1 \setminus \widehat{\mathcal{D}}_2 : \langle \mathbf{r}_3, q\mathbf{r}_{3d} \rangle = 0\} \cup \widehat{\mathcal{D}}_2$, but now $\Delta(\mathbf{x}_0) = 0$ so that $\mathbf{x} \notin \widehat{\mathcal{D}}_1$. Thus $u_{\widehat{\mathcal{D}}}^{-1}(0) = \widehat{\mathcal{D}}_2$.

In proving global attractivity of $\widehat{\mathcal{A}}$ to $\widehat{\mathcal{H}}$, we conclude from theorem 8.2 in the work of Goebel et al.[30] that each maximal solution $\mathbf{x}$ to $\widehat{\mathcal{H}}$ approaches the nonempty set that is the largest weakly invariant subset of $\widehat{V}_q^{-1}(\xi) \cap (\widehat{\mathcal{A}} \cup (\widehat{\mathcal{D}}_2 \setminus \widehat{\mathcal{D}}_1)) = \widehat{\mathcal{A}} \cup (\widehat{\mathcal{D}}_2 \setminus \widehat{\mathcal{D}}_1)$ for some $\xi \in \mathbb{R}_{\geq 0}$. Since $\widehat{\mathcal{G}}(\mathbf{x}) \subset \widehat{\mathcal{C}} \setminus \widehat{\mathcal{D}}$ for each $\mathbf{x} \in (\widehat{\mathcal{D}}_2 \setminus \widehat{\mathcal{D}}_1) \setminus \widehat{\mathcal{A}}$, we conclude global attractivity of $\widehat{\mathcal{A}}$ to $\widehat{\mathcal{H}}$.

In proving stability of $\widehat{\mathcal{A}}$ to $\widehat{\mathcal{H}}$, note that $\widehat{V}_q$ is positive definite relative to $\widehat{\mathcal{A}}$ and tends to infinity as $|\mathbf{x}|_{\widehat{\mathcal{A}}} \to \infty$ since $|\mathbf{x}|_{\widehat{\mathcal{A}}} \leq |\mathbf{x}|_{\mathcal{A}}$. Since $\widetilde{V}_q$ is independent of $(s_1, \mathbf{s}_2)$, we can rewrite $\widehat{\mathcal{A}} = \{\mathbf{x}_0 \in \mathcal{S}_{\mathbf{x}_0} : V_q(\mathbf{r}, \mathbf{z}, \mathbf{r}_3) \leq \delta\} \times \mathbb{R} \times \mathbb{R}^3$, and then there exist $\widehat{\alpha}_1, \widehat{\alpha}_2$ of class $\mathcal{K}_\infty$ such that $\widehat{\alpha}_1(|\mathbf{x}|_{\widehat{\mathcal{A}}}) \leq \widehat{V}_q(\mathbf{x}) \leq \widehat{\alpha}_2(|\mathbf{x}|_{\widehat{\mathcal{A}}})$ for each $\mathbf{x} \in \mathcal{S}_{\mathbf{x}}$ by lemma 3 from Postoyan et al.[16]

Lastly, to assert the absence of Zeno solutions to $\widehat{\mathcal{H}}$, we check the image of $\widehat{\mathcal{D}}$ under $\widehat{\mathcal{G}}$ as follows:

$$\begin{cases} \widehat{\mathcal{G}}(\widehat{\mathcal{D}}_1 \setminus \widehat{\mathcal{D}}_2) & \subset \mathcal{C}_1 \setminus \mathcal{D}_1, \\ \widehat{\mathcal{G}}(\widehat{\mathcal{D}}_2 \setminus \widehat{\mathcal{D}}_1) & \subset (\widehat{\mathcal{C}} \setminus \widehat{\mathcal{D}}) \cap \overline{\mathcal{S}_{\mathbf{x}} \setminus \widehat{\mathcal{A}}}, \\ \widehat{\mathcal{G}}(\widehat{\mathcal{D}}_1 \cap \widehat{\mathcal{D}}_2) & \subset (\mathcal{C}_1 \setminus \mathcal{D}_1) \cup (\mathcal{D}_1 \cap (\mathcal{C}_2 \setminus \mathcal{D}_2) \cap \overline{\mathcal{S}_{\mathbf{x}} \setminus \widehat{\mathcal{A}}}). \end{cases} \tag{G1}$$

By the equalities

$$\begin{cases} \widehat{\mathcal{D}} \cap (\mathcal{C}_1 \setminus \mathcal{D}_1) & = \widehat{\mathcal{D}}_2 \setminus \widehat{\mathcal{D}}_1, \\ \widehat{\mathcal{D}} \cap (\widehat{\mathcal{C}} \setminus \widehat{\mathcal{D}}) \cap \overline{\mathcal{S}_{\mathbf{x}} \setminus \widehat{\mathcal{A}}} & = \emptyset, \\ \widehat{\mathcal{D}} \cap (\mathcal{C}_1 \setminus \mathcal{D}_1) \cup \left(\mathcal{D}_1 \cap (\mathcal{C}_2 \setminus \mathcal{D}_2) \cap \overline{\mathcal{S}_{\mathbf{x}} \setminus \widehat{\mathcal{A}}} \right) & = (\widehat{\mathcal{D}}_1 \setminus \widehat{\mathcal{D}}_2) \cup (\widehat{\mathcal{D}}_2 \setminus \widehat{\mathcal{D}}_1), \end{cases} \tag{G2}$$

we have that

$$\begin{cases} \widehat{\mathcal{G}}^2(\widehat{\mathcal{D}}_1 \setminus \widehat{\mathcal{D}}_2) & \subset \widehat{\mathcal{G}}(\widehat{\mathcal{D}}_2 \setminus \widehat{\mathcal{D}}_1), \\ \widehat{\mathcal{G}}^2(\widehat{\mathcal{D}}_2 \setminus \widehat{\mathcal{D}}_1) & = \emptyset, \\ \widehat{\mathcal{G}}^2(\widehat{\mathcal{D}}_1 \cap \widehat{\mathcal{D}}_2) & \subset \widehat{\mathcal{G}}(\widehat{\mathcal{D}}_1 \setminus \widehat{\mathcal{D}}_2) \cup \widehat{\mathcal{G}}(\widehat{\mathcal{D}}_2 \setminus \widehat{\mathcal{D}}_1). \end{cases}$$

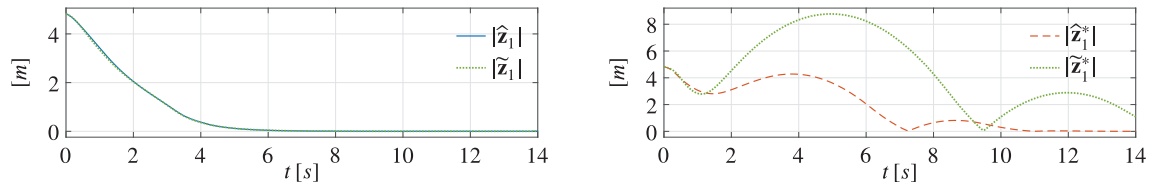

FIGURE H1 Comparison between time evolution of the norms of position errors associated with two possible solutions $\tilde{\mathbf{x}}$ and $\tilde{\mathbf{x}}^*$ using time-triggered control and that associated with two possible solutions $\hat{\mathbf{x}}$ and $\hat{\mathbf{x}}^*$ to $\widehat{\mathcal{H}}$ in (26), starting with the same initial state $\mathbf{x}(0,0)$ in (27)

In view of (G1) and (G2),

$$\begin{cases} \widehat{\mathcal{G}}^3(\widehat{D}_1 \setminus \widehat{D}_2) & = \emptyset, \\ \widehat{\mathcal{G}}^3(\widehat{D}_2 \setminus \widehat{D}_1) & = \emptyset, \\ \widehat{\mathcal{G}}^3(\widehat{D}_1 \cap \widehat{D}_2) & \subset \widehat{\mathcal{G}}(\widehat{D}_2 \setminus \widehat{D}_1). \end{cases}$$

As a result, $\widehat{\mathcal{G}}^3(\widehat{D}) \cap \widehat{D} \subset (\widehat{C} \setminus \widehat{D}) \cap \overline{\mathcal{S}_{\mathbf{x}} \setminus \widehat{\mathcal{A}}} \cap \widehat{D} = \emptyset$. Therefore, $\widehat{\mathcal{G}}^k(\widehat{D}) \cap \widehat{D} = \emptyset$ for each $k \in \{3, 4, \dots\}$ and the desired conclusion follows then from Lemma 2. ∎

APPENDIX H

We compare the performance of the event-triggered controller in Section 4.4 with a time-triggered controller that issues periodic samplings of actuation signals. Starting from the same initial condition $\mathbf{x}(0,0)$ in (27), let $\tilde{\mathbf{x}}$ and $\tilde{\mathbf{x}}^*$ denote two possible solutions using the time-triggered controller, where $\tilde{q}(t,j) = \widehat{q}(t,j)$ for each $(t,j) \in \operatorname{dom} \tilde{\mathbf{x}}$ and $\tilde{q}^*(t,j) = \widehat{q}^*(t,j)$ for each $(t,j) \in \operatorname{dom} \tilde{\mathbf{x}}^*$. For our purpose, it is reasonable to let $\overline{\Delta}_T$ and $\overline{\Delta}_T^*$ to be the average inter-event times for the solutions $\hat{\mathbf{x}}$ and $\hat{\mathbf{x}}^*$ of Section 5.2before entering the set $\widehat{\mathcal{A}}$, namely,

$$\overline{\Delta}_T := \frac{\inf\{t : \exists (t,j) \in \operatorname{dom} \hat{\mathbf{x}}, \hat{\mathbf{x}}(t,j) \in \widehat{\mathcal{A}}\}}{\inf\{j : \exists (t,j) \in \operatorname{dom} \hat{\mathbf{x}}, \hat{\mathbf{x}}(t,j) \in \widehat{\mathcal{A}}\}} \approx 0.1091 \text{ s}, \quad \overline{\Delta}_T^* := \frac{\inf\{t : \exists (t,j) \in \operatorname{dom} \hat{\mathbf{x}}^*, \hat{\mathbf{x}}^*(t,j) \in \widehat{\mathcal{A}}\}}{\inf\{j : \exists (t,j) \in \operatorname{dom} \hat{\mathbf{x}}^*, \hat{\mathbf{x}}^*(t,j) \in \widehat{\mathcal{A}}\}} \approx 0.1416 \text{ s}.$$

For simplicity, we only compare time evolution of the position error presented in Figure H1. Although the time evolution patterns for $|\tilde{\mathbf{z}}_1|$ and $|\hat{\mathbf{z}}_1|$ bear little difference, it is obvious that $|\tilde{\mathbf{z}}_1^*|$ converges slower than $|\hat{\mathbf{z}}_1^*|$. This comparison shows the effectiveness of event-triggered control in stabilizing task with an average frequency of sampling that may cause slower rate of convergence using a time-triggered controller. Furthermore, the convergence of errors using event-triggered control is guaranteed while that using time-triggered control may not be.